

EXPLORING QUANTUM WELLS IN OLED TECHNOLOGIES: A COMPREHENSIVE REVIEW OF APPLICATIONS AND ADVANCEMENTS

LILIA DEVA¹, PAVLO STAKHIRA^{1*}, VOLODYMYR FITIO¹, RUSLANA GUMINILOVYCH²,
TETIANA BULAVINETS¹, MARIIA STANITSKA^{3,4}, DMYTRO VOLYNIUK³

¹Department of Electronic Engineering, Institute of Telecommunications, Radioelectronics and Electronic Engineering, Lviv Polytechnic National University, 12 Bandera Street, 79013 Lviv, Ukraine

²Department of Physical, Analytical, and General Chemistry, Institute of Chemistry and Chemical Technologies, Lviv Polytechnic National University, 12 Bandera Street, 79013 Lviv, Ukraine

³Department of Polymer Chemistry and Technology, Kaunas University of Technology, Baršausko 59, 51423 Kaunas, Lithuania

⁴Ivan Franko National University of Lviv, Universytetska Str. 1, 179000 Lviv, Ukraine

*Corresponding author: pavlo.y.stakhira@lpnu.ua

Received: 19.12.2024

Abstract. Efficient organic light-emitting diodes (OLEDs) with structurally integrated quantum wells are attracting considerable attention due to their ability to obtain narrow spectral radiation and high radiation efficiency. In particular, there is a tendency to enhance efficiency in such light-emitting devices due to the inclusion in their architecture of phosphorescent metal-organic complexes and materials with an inherent mechanism of thermally activated delayed fluorescence. Due to strong spin-orbit interaction, this approach transforms non-radiating triplet excitons into radiating singlet excitons. In this review, we mainly discuss the mechanisms of electrogenerated exciton localization in potential wells to preserve OLED efficiency with increased emission brightness and reduced exciton leakage channels, report on quantum wells design strategies for OLEDs exhibiting blue, green, red, infrared, and white highly efficient radiation, and provide information on the practical application of quantum well technology in various organic electronics devices. By analyzing recent developments and challenges, this comprehensive review provides insights into the potential of quantum wells to revolutionize OLED innovation and future trends.

Keywords: organic light-emitting diode, quantum well, electroluminescence, thermally activated delayed fluorescence

UDC: 535.37; 621.38

DOI: 10.3116/16091833/Ukr.J.Phys.Opt.2025.02001

1. Introduction

In recent years, organic light-emitting diodes (OLEDs) have become an essential element of modern lighting due to their ability to provide bright, energy-efficient radiation. Thanks to materials science and engineering innovations, OLEDs have revolutionized the electronics and display industries, offering solutions for thin, light, and high-performance devices. Unlike traditional liquid crystal displays, which require backlighting, OLEDs can emit light independently, significantly reducing power consumption and providing deeper black levels. It has contributed to adopting OLEDs in producing displays for smartphones, TVs, and portable gadgets, where image quality and energy efficiency are essential [1, 2]. Thus, OLEDs occupy a crucial position in modern display and lighting technology, actively influencing the electronics, communications, and energy-efficient industries. Their unique ability to generate high-quality images with low power consumption makes them indispensable for medical sensors, as well as for flexible screens and portable devices [3, 4]. However, despite

significant progress in this field, there are still challenges related to their effectiveness and lifetime. The development of OLED technologies often faces fundamental limitations, such as low internal quantum efficiency and the problem of material degradation during long-term operation.

In this context, quantum wells (QWs) have attracted considerable attention from the scientific community. The idea of quantum wells is based on creating ultrathin layers where electrons and holes are confined in one-dimensional space. This phenomenon makes it possible to significantly strengthen control over the energy states of particles and create narrow energy levels, which helps reduce energy losses and increase radiation efficiency. Such structures were successfully used in semiconductor lasers and LEDs for the first time, providing greater efficiency and operation stability. Now, similar principles are being tried to be adapted to OLED [5, 6].

Integrating quantum wells into OLEDs opens up new possibilities for achieving higher brightness and longevity, mainly through improved exciton confinement and reduced probability of their uncontrolled scattering. Due to the confinement of charges in QW structures, the likelihood of recombination with radiation increases significantly, which is especially relevant for high-quality displays with a large color spectrum. In addition, quantum wells make it possible to create OLEDs with stable color rendering, a prerequisite for applications in professional graphics, medical equipment, and other industries where color accuracy is critical [7, 8].

Multilayer QW structures (MQW) allow for the creation of OLEDs with different thicknesses of active layers, which helps optimize energy transfer between materials. They also allow for controlling the intensity and quality of emitted light, which is essential for applications in lighting systems with high requirements for color stability and energy efficiency [9]. In addition, using quantum wells can significantly reduce the cost of OLED production since such structures reduce the required materials without losing performance.

A significant breakthrough in the research of quantum wells in OLEDs has come about thanks to the work of scientists who discovered that integrating QW structures can significantly improve the internal quantum efficiency of OLEDs. For example, a study by W. Chen et al. [10] demonstrated that quantum wells can increase the internal quantum emission factor due to more efficient confinement of excitons in thin layers of the active region. They have achieved significant results in improving the stability and brightness of OLEDs, especially in the blue emission spectrum, where there are traditionally difficulties in maintaining stability. This approach made it possible to extend the service life of blue OLEDs almost twice compared to traditional structures.

Other research groups have drawn attention to the ability of quantum wells to reduce heat loss in OLEDs, which is one of the main factors causing the degradation of organic materials. A study by K. Kim et al. [11] showed that using multilayer QW structures allows for better thermal control due to the adequate confinement of charge carriers. They demonstrated that OLEDs with QW structures have less heat loss, contributing to more stable device operation and improved energy efficiency. It has opened new opportunities for using OLEDs in high-pixel-density devices and flexible displays that require maximum energy efficiency [12]. In addition, research by S.W. Park et al. [13] contributed significantly to understanding energy transfer mechanisms in OLEDs with QW structures. Their experiments showed that quantum wells can substantially

reduce the probability of uncontrolled recombination of excitons due to precise tuning of energy levels. It helped to achieve a high coefficient of external quantum efficiency and better quality radiation without unwanted color changes during long-term operation.

Despite the significant advantages of quantum wells in semiconductor devices, applying these structures in OLEDs is at the active research stage. As noted, QWs can significantly reduce losses due to uncontrolled energy dissipation and increase the lifetime of excited states, thereby contributing to more efficient emissions. It makes further research on quantum wells an important step for developing next-generation OLEDs to meet industries' energy efficiency and durability requirements [14].

However, along with the advantages, OLEDs have significant limitations. Each spectral range of colors – blue, green, red, and white – has unique challenges. For example, blue OLEDs have a significantly shorter lifespan than red and green, rapidly degrading color balance over time. Maintaining high quantum efficiency is also challenging, as organic materials are prone to degradation under high temperatures and prolonged exposure. It has become a key challenge for engineers and researchers seeking to find effective methods to improve the stability and performance of OLEDs without compromising their unique characteristics [15, 16]. Studies show that applying quantum wells can significantly reduce these losses by more effectively confining excitons in blue OLEDs, allowing them to maintain stable brightness and color accuracy over a long period of operation [17]. Green OLED is one of the most efficient in energy consumption and operation duration, making it a central component in most display technologies. However, engineers still face difficulties fine-tuning the emission so that the green OLED is optimally aligned with the blue and red to form a quality color spectrum. A study by Zh. Kou et al. [18] showed that a green OLED's stability and emission quality can be improved using quantum wells. This is suitable for creating displays used in professional photo and video processing, games, and augmented reality, where color accuracy is critical [19]. Infrared (IR) OLEDs have essential applications in industries that require unique optical properties, including night vision devices, medical equipment, remote sensors, and temperature monitoring devices. Due to their high resolution and limited visibility conditions, they are used for health monitoring, non-contact temperature measurement, and diagnostics. Radiation stability in the long-wave spectrum is essential since maintaining an accurate infrared signal is critical for medical and military devices [20, 21]. White OLEDs are particularly important for lighting systems due to their high energy efficiency and ability to produce a wide range of colors closer to natural daylight. They are widely used in indoor and outdoor lighting, interior design, architectural lighting, and the automotive industry, especially in environments where light quality is essential, such as medical and educational facilities. One of the challenges of white OLEDs is maintaining color uniformity over time. Studies by W. Zhao et al. and Y. Zhou et al. have demonstrated that introducing QW structures avoids these changes, maintaining color uniformity by effectively limiting the movement of charge carriers [22, 23].

This review offers a comprehensive analysis of the current advances in the use of quantum wells in OLED technologies based on the latest experimental data and theoretical models, demonstrating the significant potential of these structures for developing the OLED industry. It is also aimed at identifying the main trends in this direction and evaluating the prospects for applying quantum wells to improve the performance of OLEDs, especially given the industrial requirements for the devices' quality, energy efficiency, and durability. The

main focus is on QWs - OLEDs based on low molecular weight organic semiconductors, which show significant advantages in optical and electrical characteristics. The work results highlight the benefits of QWs for each spectral range. They also expand our knowledge about QW structures and show that their application can significantly extend the capabilities of OLED technologies, making them more adaptable to the needs of different market segments and technological challenges.

2. Review process

Through an extensive review of four databases (Scopus, Web of Science, Google Scholar, and ResearchGate), 4120 relevant studies were initially identified. The extracted data were organized in a Microsoft Excel spreadsheet, and duplicate entries were removed. The data extraction focused on study characteristics and bibliographic details, including the first author and the year of publication.

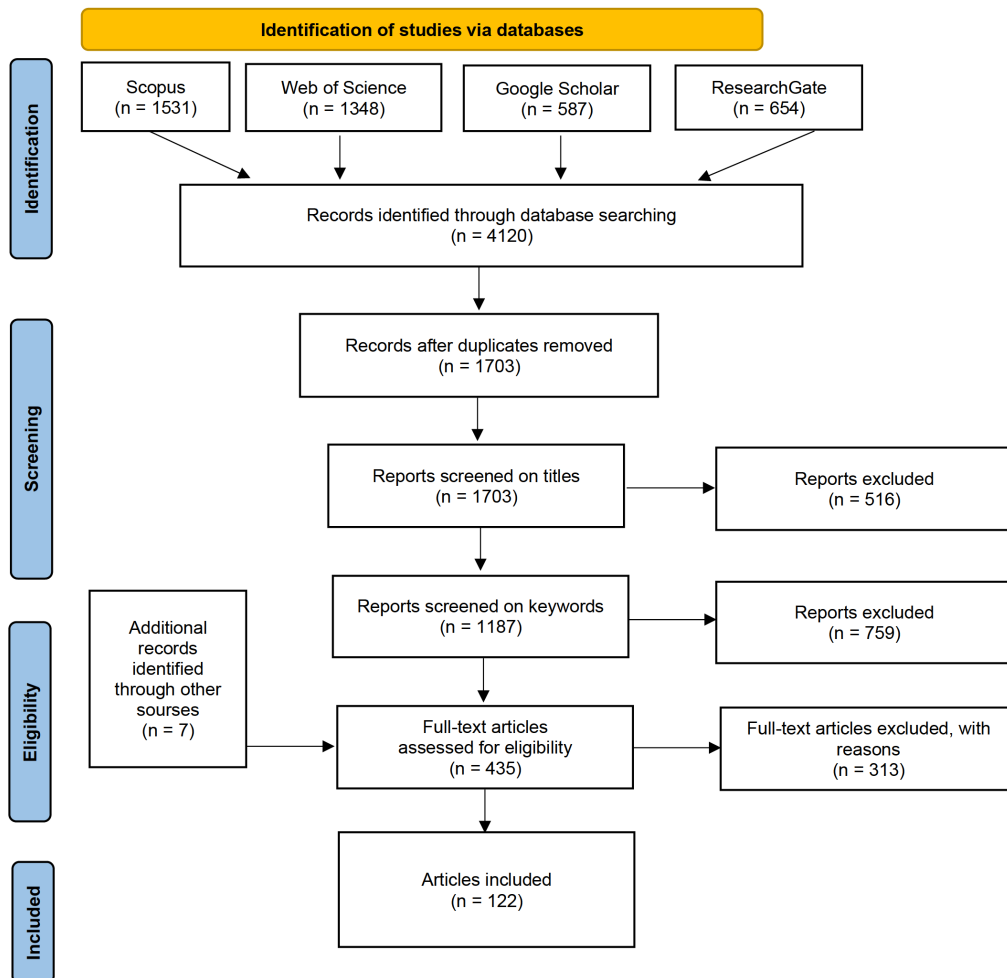


Fig. 1. Flow diagram of the review process.

After eliminating duplicates, 1703 unique records remained. These records underwent title screening, resulting in the exclusion of 516 studies. Subsequently, a keyword-based screening process excluded an additional 759 studies. Seven more records were identified through alternative sources. Ultimately, 435 full-text articles were selected for detailed analysis.

After further review of these full texts, 313 articles were excluded for various reasons (limited methodological reliability or insufficient information on electroluminescence mechanisms and quantum well design), leaving 122 articles for the final inclusion list. The selection process prioritized criteria such as relevance, scientific validity, and the recency of information. The manuscript emphasizes electroluminescence mechanisms and quantum well designs, which are pivotal for enhancing brightness and minimizing energy losses in modern OLED devices. Fig. 1 outlines the study selection process.

3. Theoretical modeling of energy levels and optimization of exciton containment mechanisms in a quantum well

Quantum wells are nanoscale semiconductor structures that can localize excitons, which increases radiation efficiency and allows reaching a narrow spectral range. Studies show that using organometallic complexes in combination with materials exhibiting thermally activated delayed fluorescence opens up new opportunities for increasing the OLED's performance. The use of these materials helps to convert triplet excitons into singlet ones, thereby ensuring high radiation efficiency. Such properties are characteristic of inorganic light-emitting heterostructures based on quantum wells (QWs), small-sized heterosystems with their inherent exciton states [24]. A structural feature of such quasi-two-dimensional (2D) heterostructures is the presence of a narrow-band emitter layer, the thickness of which is approximately equal to the Bohr radius of the exciton (less than 10 nm) [25]. This layer is placed between two wide-gap semiconductor layers of nanoscale thickness. A schematic presentation of such 2D- heterostructures is shown in Fig. 2, where d is the thickness of a narrow-band emitter layer.

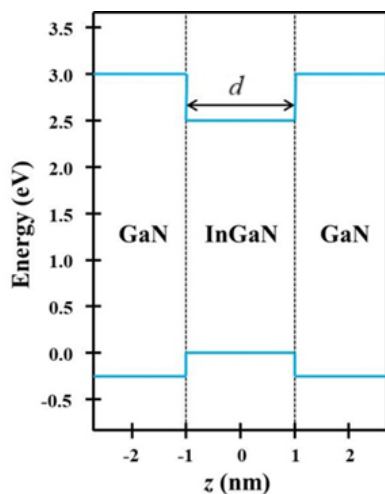


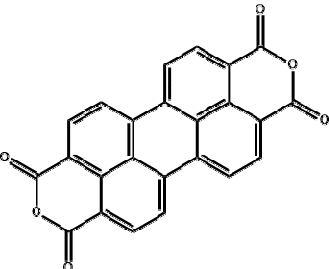
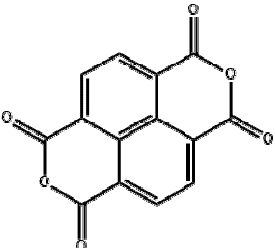
Fig. 2. Quasi-two-dimensional (2D) inorganic heterostructure with a narrow-band emitter layer of thickness d .

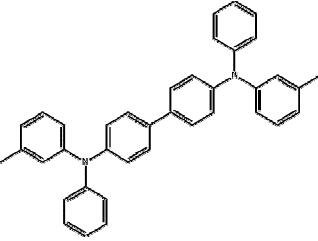
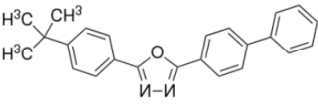
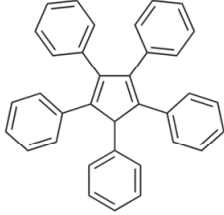
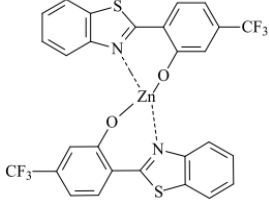
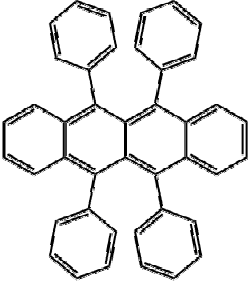
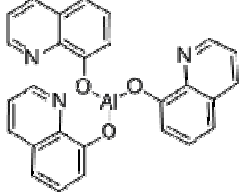
It is energetically favorable for electrons and holes to localize in the potential well with such a configuration, as shown in Fig. 2. In contrast, the effective distance between the electron and the hole (exciton) decreases. Therefore, the binding energy of the exciton increases. Using such a design of heterostructure devices made it possible to increase the binding energy of excitons localized in 2D quantum wells to values that significantly exceed the thermal energy at room temperature. The practical implementation of this concept first enabled the creation of inorganic heterostructural LEDs operating at room temperature and, later, semiconductor lasers [5]. At the same time, a decrease in the density of exciton states

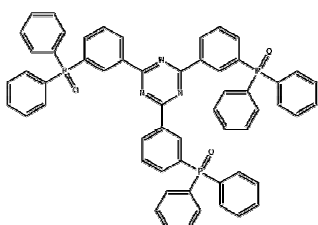
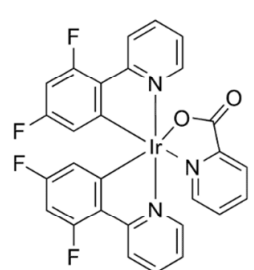
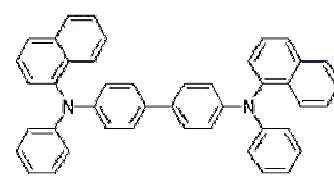
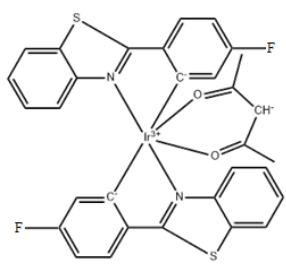
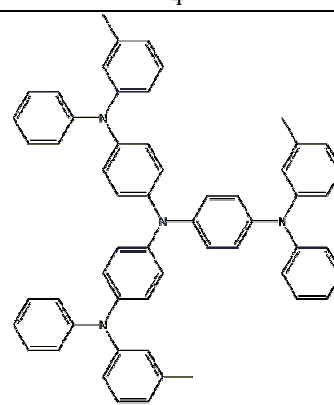
in such optoelectronic devices resulted in low threshold voltage values and a high electroluminescence quantum yield (ELQY). Note that light-emitting devices on quantum wells are the basic elements of modern telecommunication networks [26-29]. Since developing OLED structures with a transport and emission layer [30, 31], many efforts have been directed at increasing their efficiency. The synthesis of new effective functional materials, including transport and emitting materials, research of emission mechanisms, and development of new OLED structures, particularly quantum wells and superlattice structures, is being carried out. Both monochrome and white OLEDs were formed based on QWs [32-36]. A list of the primary organic semiconductor materials used in the functional layers of light-emitting diodes with a structure of quantum wells (QW-OLEDs) considered in this review is given in Table 1.

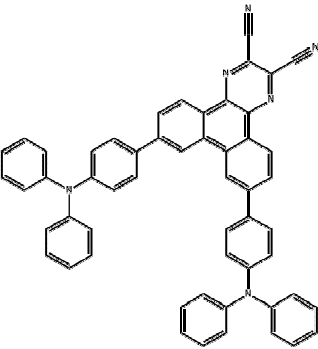
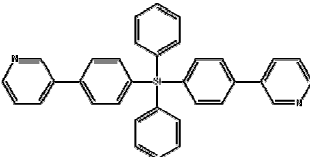
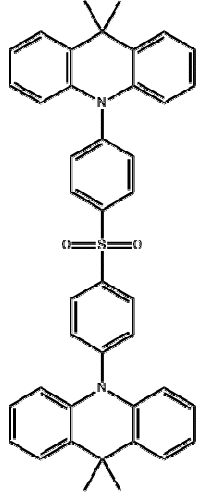
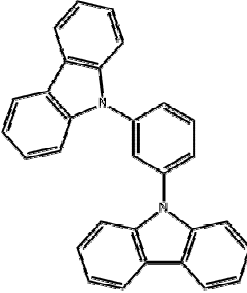
Quantum wells are generally divided into type I and type II configurations. In a type I QW structure, materials with a wide band gap overlap with materials with a narrow band gap. Thus, in a structure with type I QW structure, both carriers are localized in the potential well layer due to a barrier layer. Meanwhile, the potential well and potential barrier energy levels (PBL) alternate in a type II QW structure, and electrons and holes accumulate in different molecules. However, the device's architecture, the type of materials used in the quantum well structures, and the width of the quantum well have a decisive effect on improving the device's efficiency.

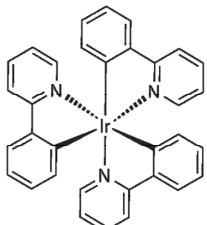
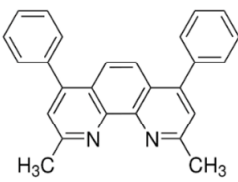
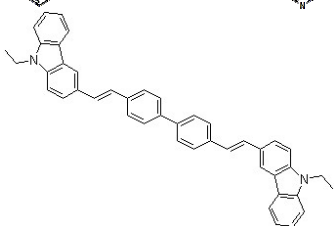
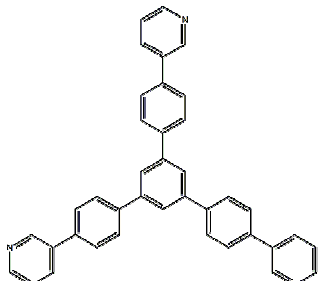
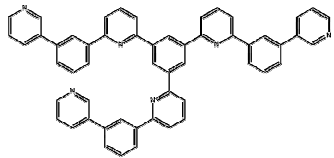
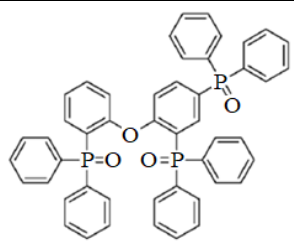
Table 1. List of organic semiconductor materials used in QW-OLED functional layers.

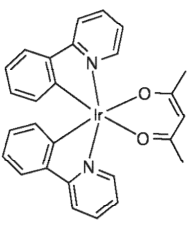
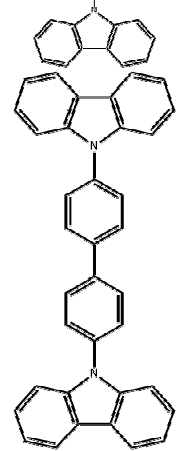
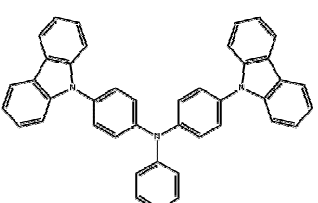
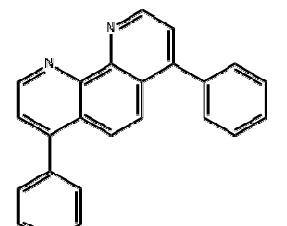
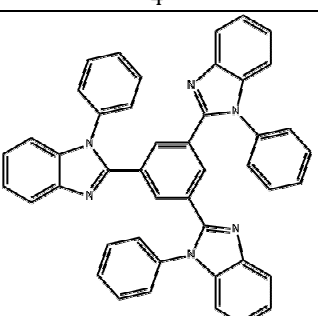
Abbreviation	Chemical nomenclature	Molecular formula	Chemical structure	HOMO/LUMO, eV	Ref.
1	2	3	4	5	6
PTCDA	3,4,9,10 perylenetetracarboxylic dianhydride	C ₂₄ H ₈ O ₆		6.9 / 2.2	[36]
NTCDA	3,4,7,8-Naphthalenetetracarboxylic dianhydride	C ₁₄ H ₄ O ₆		7.2 / 3.1	[36]

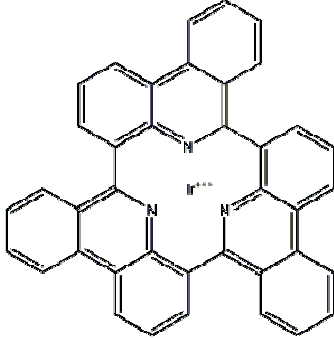
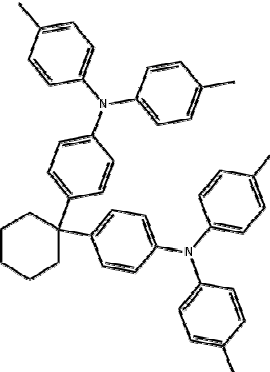
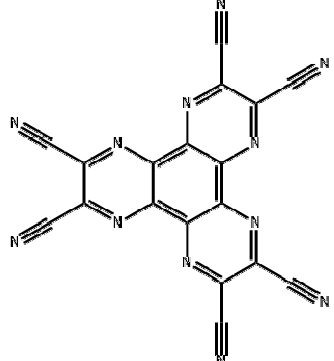
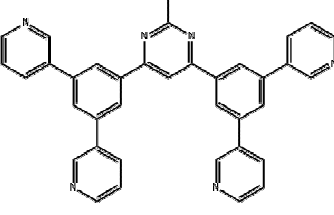
1	2	3	4	5	6
TPD	N, N'-diphenyl-N, N'-bis-(3-methylphenyl)-[1,1'-biphenyl]-4, 4'-diamine	$C_{38}H_{32}N_2$		5.5 / 2.3	[37, 42, 43]
t-BuPBD	2-(4-Biphenyl)-5-(4-tert-butylphenyl)-1,3,4-oxadiazole	$C_{24}H_{22}N_2O$		6.1 / 2.7	[42]
PPCP	1,2,3,4,5-pentaphenyl-1,3-cyclopentadiene	$C_{35}H_{26}$		5.6 / 2.8	[42]
Zn(4-TfmBTZ)₂	2-(4-trifluoromethyl-2-hydroxyphenyl)benzothiazole) zinc	$C_{27}H_{18}AlN_3O_3$		5.83 / 2.99	[41]
Rubrene	5,6,11,12-tetraphenyltetracene	$C_{42}H_{28}$		5.4 / 3.2	[38]
Alq₃	Tris(8-hydroxyquinoline) aluminum	$C_{27}H_{18}AlN_3O_3$		5.62 / 2.85	[37, 38, 39, 40, 41, 42]

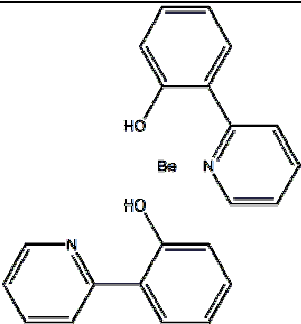
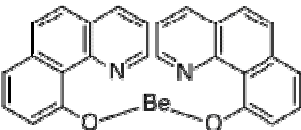
1	2	3	4	5	6
PO-T2T	FIrPic (Ir(diFppy)₂(pic))	NPB	(F-BT)₂Ir(acac)	m-MTDATA	
2,4,6-tris[3 (diphenylphosphiny) phenyl]- 1,3,5-triazine	Bis[2-(4,6-difluorophenyl) pyridinato- C2,N](picolinato)iridium	N,N'- di(naphthalene- 1-yl)-N,N'- diphenyl- benzidine	Bis(2-(2-fluorophenyl)-1,3- benzothiazolato- N,C ²)iridium(acetylacetonate)	4,4',4''-Tris[(3- methylphenyl)phenylamino]triphe- nylamine	
C₅₇H₄₂N₃O₃P₃	C₂₈H₁₆F₄IrN₃O₂	C₄₄H₃₂N₂	C₅₇H₄₈N₄		
					
7.55 / 3.50	5.8 / 3.1	5.5 / 2.4	5.8 / 3.4	5.1 / 2.0	[43]
[46]	[17, 45, 46]	[17, 38, 39, 40, 41, 44]	[43]	[43]	

1	2	3	4	5	6
TPA - DCPP	7,10-bis(4-(diphenylamino) phenyl)-2,3-dicyanopyrazino-phenanthrene	$C_{54}H_{34}N_6$		5.3 / 3.5	[48]
DPPS	Diphenyl-bis(4-(pyridin-3-yl)phenyl)silane	$C_{34}H_{26}N_2Si$		6.5 / 2.5	[47]
DMAC-DPS	10,10'-(4,4'-Sulfonylbis(4,1-phenylene))bis(9,9-dimethyl-9,10-dihydroacridine)	$C_{42}H_{36}N_2O_2S$		5.92 / 2.92	[47]
mCP	N,N'-Dicarbazolyl-3,5-benzene (1,3-Bis(N-carbazolyl)benzene)	$C_{30}H_{20}N_2$		5.9 / 2.4	[17, 45, 46, 47, 48]

1	2	3	4	5	6
Ir(ppy)₃	Tris[2-phenylpyridine-C _{2,n}]iridium(III)	C ₃₃ H ₂₄ IrN ₃		5.6 / 3.0	[44, 49]
BCP	2,9-Dimethyl-4,7-diphenyl-1,10-phenanthroline (Bathocuproine)	C ₂₆ H ₂₀ N ₂		6.4 / 2.9	[39, 49]
BCzVBi	4,4'-Bis(9-ethyl-3-carbazovinylene)-1,1'-biphenyl	C ₄₄ H ₃₆ N ₂		5.4 / 2.5	[49]
TmPyPB	1,3,5-Tri(m-pyrid-3-ylphenyl)benzene	C ₃₉ H ₂₇ N ₃		6.75 / 2.75	[17, 48]
Tm3PyP26PyB	1,3,5-Tris(6-(3-(pyridin-3-yl)phenyl)pyridin-2-yl)benzene	C ₅₄ H ₃₆ N ₆		6.5 / 2.9	[48]
DPETPO	2,2',4-tris (di(phenyl)-phosphoryl)-diphenylether			6.4 / 2.7	[48]

1	2	3	4	5	6
Ir(ppy)₂acac	CBP	TCTA	BPhen	TPBi	
Bis(2-phenylpyridine)(acetylacetonate)iridium(III)	4,4'-Bis(N-carbazolyl)-1,1'-biphenyl	4,4',4''-Tris(carbazol-9-yl)triphenylamine	Bathophenanthroline (4,7-Diphenyl-1,10-phenanthroline)	2,2',2''-(1,3,5-Benzinetriyl)-tris(1-phenyl-1-H-benzimidazole)	
$C_{27}H_{23}IrN_2O_2$	$C_{36}H_{24}N_2$	$C_{54}H_{36}N_4$	$C_{24}H_{16}N_2$	$C_{45}H_{30}N_6$	
					
5.5 / 3.0	6.0 / 2.9	5.83 / 2.43	6.4 / 3.0	6.2 / 2.7	
[50]	[43, 44, 46, 49, 51]	[17, 43, 44, 50, 51]	[43, 45, 49]	[43, 44, 45, 49]	

1	2	3	4	5	6
Ir(piq)₃	TAPC	HAT-CN	B3PyMPM		
Tris(1-phenylisoquinoline)iridium(III)	1,1-Bis[(di-4-tolylamino)phenyl]cyclohexane	1,4,5,8,9,11-Hexaazatriphenylenehexacarbonitrile	4,6-Bis(3,5-di-3-pyridinylphenyl)-2-methylpyrimidine		
$C_{45}H_{30}IrN_3$	$C_{46}H_{46}N_2$	$C_{18}N_{12}$	$C_{37}H_{26}N_6$		
					
5.1 / 3.1	5.5 / 2.0	9.5 / 4.4	6.97 / 3.53		
[49, 51]	[48, 50]	[48, 50]	[50]		

1	2	3	4	5	6
Bepp2	bis[2-(2-hydroxyphenyl)-pyridine] beryllium	$C_{22}H_{16}BeN_2O_2$		5.7 / 2.6	[51]
Bebp2	Bis(10-hydroxybenzo[h]quinolinato) beryllium	$C_{26}H_{16}BeN_2O_2$		5.5 / 2.8	[51]

Evidence of exciton quantum confinement in organic QWs structures was first provided by F.F. So and S.R. Forrest [36], who fabricated and later investigated several highly ordered organic QWs based on PTCDA and NTCDA using molecular beam epitaxy under ultra-high vacuum conditions. It is worth noting that highly ordered thin nanoscale organic films were formed on non-crystalline substrates, enabling the design of organic heterostructures with a wide spectrum of layer combinations without considering the matching of crystal lattices, as required for inorganic heterostructure devices. Analyzing structures with PTCDA/NTCDA quantum wells and using optical absorption and time-resolved photoluminescence techniques, the authors concluded that the binding energy of excitons increases with decreasing well width while the exciton lifetime decreases.

It is widely acknowledged that achieving high quantum efficiency and high-quality light emission in OLEDs is a challenging problem that requires a comprehensive solution [52-55]. It is necessary to ensure efficient charge carrier injection, balanced hole, and electron transport, exciton localization in the emitting zone, and efficient excitonic recombination with subsequent light extraction. In this regard, using OLED structures with embedded quantum wells has proven to be a successful technological solution for improving the characteristics of organic light-emitting diodes, including obtaining narrower spectral emission and higher emission efficiency [37, 56-58]. Authors of [37] conducted a comparative analysis of the recombination efficiency of OLEDs with QWs based on Alq₃ and TPD with alternative multilayer organic light-emitting diodes with multi-QW structures based on TPD/Alq₃. The main light characteristics of OLEDs with QWs series were better than those of OLEDs with a single QW. This effect is obviously associated with an increase in carrier concentration in the emitting zone of cascade QWs. Similar conclusions were drawn in other studies [57, 58].

In OLED structures, the processes of charge carrier injection and transport are significant factors affecting device light emission performance, as they determine the electron-hole balance in the emitting layer. Imbalance in electron and hole flows into the

emitting layer leads to increased dark current, high turn-on voltage, and consequently, a decrease in the effective operating lifetime of organic light-emitting diodes [59-63]. At least two factors complicate solving this problem: different electron and hole mobilities in transport layers and existing energy barriers at the anode/ hole transport layer (HTL) and electron transport layer (ETL)/cathode interfaces. In [64], OLEDs with different sets of alternating quantum well structures based on MoO₃/TPD were investigated. In these devices, the hole injection layer (HIL) decreases due to the formation of an interfacial dipole interface between the inorganic n-type semiconductor MoO₃ layer and the indium tin oxide (ITO) anode layer [65]. Absorption spectra show that thin films of MoO₃ and TPD are transparent to the green light emitted in the Alq₃ layer. In structures with quantum wells, such as HIL/HTL, lower voltage values were observed, as well as improvements in brightness characteristics and energy efficiency compared to OLED structures without quantum wells.

In [38], the characteristics of electric carriers' transport in OLEDs with quantum wells were modeled, and the influence of the well width and the quantum well number on carrier distribution in the electric field and recombination rate was investigated. NPB was used as the HTL, Alq₃ as the potential barrier and ETL, and Rubrene as the potential well. These organic layers were placed between a LiF/Al cathode and an ITO anode to ensure efficient carrier injection. The layer-by-layer structure of such a device with multiple quantum wells is shown in Fig. 3a.

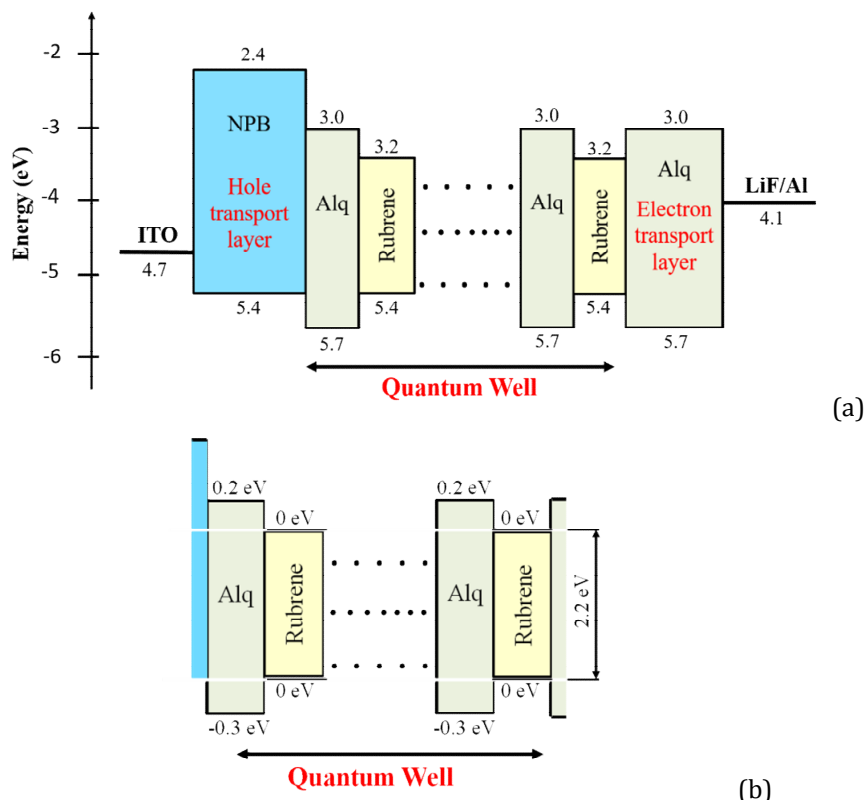


Fig. 3. (a) Schematic energy diagrams of MQW OLEDs [38] [Chan, J., Lu, A. W., Ng, A. M. C., Djurić, A. B., & Rakić, A. D. (2006). Organic quantum well light-emitting diodes. *Proceedings of SPIE*, 6038, Photonics: Design, Technology, and Packaging II, 60381M. Permission conveyed through CCC Marketplace]. (b) Discrete energy levels diagram of electrons and holes for a simple MQW-OLEDs substructure.

This study investigated charge carrier transport (electrons and holes) using the continuity and Poisson's equations. A self-consistent solutions allow for finding the electron density n , hole density p , and potential Ψ using the semiconductor solver Atlas [66]. The recombination rate of charge carriers for devices with single, double, and triple QW based on Alq₃ was also modeled. It was established that recombination is possible in all OLED layers, but the maximum recombination rate is achieved in the leftmost quantum well. According to [38], such a structure's theoretical prediction characteristics results align well with experimental results.

To determine the discrete energy levels of electrons and holes in the structure depicted in Fig. 3a, it was divided into three substructures, as shown in Fig. 3b, and the potential barrier heights were recalculated accordingly. Based on the upper substructure, discrete electron energy levels E_e can be found. The lower structure determines the bandgap width which, in this case, is $E_g=2.2$ eV. In this study, authors identified discrete energy levels for holes E_h , which take negative values, for the lowest structure. The energy difference between electrons and holes is expressed as follows:

$$\Delta E = E_e + E_g - E_h, \quad (1)$$

ΔE will approximately determine the frequency of light-emitting structure generation.

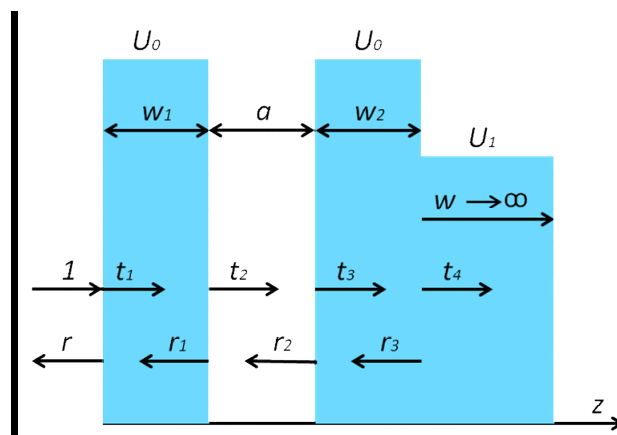


Fig. 4. Dependence of the nanostructure potential energy on the z coordinate. The two potential barriers of height U_0 and widths w_1 and w_2 , respectively, form a potential well, the width of which is equal to a . A plane de Broglie wave with unit amplitude falls onto the structure; t_j are the amplitudes of waves propagating to the right, and r_j are the amplitudes of waves propagating to the left.

Thus, the problem arises: by what method can the energy levels of electrons (holes) for corresponding quantum wells be calculated? In the case where the barriers have an infinite width, finding the discrete energy levels and corresponding wave functions is described in almost all textbooks on quantum mechanics [67]. However, if the barriers have finite width, finding the energy levels in potential wells and their corresponding wave functions becomes more complicated. A relatively simple method of finding energy levels for quantum wells with finite barrier width is proposed in [68]. By analogy, this method is used to solve the quantum structure shown in Fig. 3b, the results shown in Fig. 4. In this structure, on the left, we have a potential barrier with a height U_0 and a width w_1 , while on the right, we have two barriers: a height U_0 and a width w_2 and a barrier with a height U_1 extending to positive infinity. In this method, a de Broglie wave of unit amplitude is considered to be incident on

the structure. The amplitudes t_j and r_j are determined from the continuity condition of the wave function and its first derivative at the boundary of potential energy change. Respectively, we obtain two equations: one for the wave function and another for its derivative. Since there are four boundaries of potential energy change according to Fig. 4, we end up with a linear inhomogeneous algebraic system of eighth-order equations, where t_j and r_j are the unknowns.

A plane de Broglie wave of unit amplitude, describing the motion of a particle with energy E , falls on the first barrier from left to right. The plane wave equation is as follows:

$$\psi_1(z) = \exp(ik_0z), \quad (2)$$

where $k_0 = \sqrt{2mE/\hbar^2}$, m - effective particle mass, $\hbar = h/2\pi$ - reduced Planck's constant.

A wave with amplitude r is reflected from the first barrier, which is a complex quantity:

$$\psi_r(z) = r \exp(-ik_0z). \quad (3)$$

Similarly, we will describe de Broglie plane waves for other segments:

$$\psi_{t_j}(z) = t_j \exp(ik_jz), \quad \psi_{r_j}(z) = r_j \exp(-ik_jz), \quad (4)$$

where $k_1 = \sqrt{2m(E-U_0)/\hbar^2}$, $k_2 = k_0$, $k_3 = k_1$, $k_4 = \sqrt{2m(E-U_1)/\hbar^2}$.

Taking into account Eqs. (1-4), and satisfying the continuity condition for each potential energy gap, we can write an inhomogeneous system of eighth-order linear algebraic equations:

for the first potential energy gap:

$$\begin{cases} 1 + r = t_1 + r_1 \exp(ik_1w_1), \\ ik_0 - ik_0r = ik_1t_1 - ik_1r_1 \exp(ik_1w_1), \end{cases}$$

for the second potential energy gap:

$$\begin{cases} t_1 \exp(ik_1w_1) + r_1 = t_2 + r_2 \exp(-ik_0a), \\ ik_1t_1 \exp(ik_1w_1) - ik_1r_1 = ik_0t_2 - ik_0r_2 \exp(-ik_0a), \end{cases}$$

for the third potential energy gap:

$$\begin{cases} t_2 \exp(ik_0a) + r_2 = t_3 + r_3 \exp(ik_1w_2), \\ ik_0t_2 \exp(ik_0a) - ik_0r_2 = ik_0t_3 - ik_1r_3 \exp(ik_1w_2), \end{cases}$$

for the fourth potential energy gap:

$$\begin{cases} t_3 \exp(ik_1w_2) + r_3 = t_4, \\ ik_1t_3 \exp(ik_1w_2) - ik_1r_3 = ik_4t_4. \end{cases}$$

Thus, finding t_j and r_j is reduced to solving a linear system of algebraic equations with a right-hand non-zero part, and the number of such equations in the system equals twice the number of potential energy gaps.

All wave numbers k_j depend on the resonance energy E , which we need to find. Additionally, t_j and r_j also depend on E . The maximum of the wave function will be observed in the quantum well, so by plotting the dependence of the module $t_2(E)$ or $r_2(E)$, we can find resonant energy levels.

The dependence of $t_2(E)$ for parameters $U_0=U_1=0.056$ eV, $m=0.2m_e$, $w_1=2.5$ nm, $a=8$ nm is shown in Fig. 5. As we can see, $|t_2(E)|$ sharply increases at certain values of E .

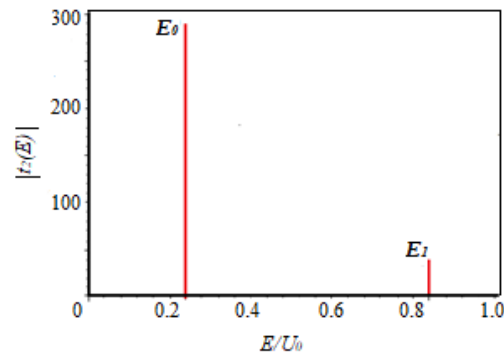


Fig. 5. Dependence of the amplitude t_2 in the quantum well on the particle energy.

Two resonant energy levels were obtained for such data: $E_0=0.2391U_0$ and $E_1=0.8388U_0$. At resonant energy levels, the de Broglie wave amplitude sharply increases. Thus, it is possible to find resonant energy levels in Fig. 3b for the upper and lower quantum wells. And by $|t_j(E)|^2$ or $|r_j(E)|^2$, it is possible to conclude the probability of finding charge carriers in the quantum wells.

4. Features of the architecture of QWs – OLEDs with different color emission

QWs – OLEDs provide a broad spectrum of color emission due to the possibility of fine-tuning the architecture of quantum wells. Changing the parameters of such structures, particularly the width of the quantum wells and the materials of the barrier and emitter layers, makes it possible to obtain highly efficient devices emitting in different color ranges. An essential factor is that the quantum wells limit the movement of electrons and holes in the direction perpendicular to the layer, which leads to quantum effects. The emission spectrum can be precisely adjusted by changing the size of the quantum wells, which determines the transit energy of the charge carriers and, accordingly, the emission wavelength. As a result, OLEDs based on QWs can emit light in a wide range, creating devices with high brightness, color saturation, and stability. The different emission colors in OLEDs, such as blue, green, red, and white, require specific quantum well design approaches to achieve optimal performance. An important feature is also the high efficiency of conversion of electrical energy into light while maintaining thermal stability, which is essential for attaining durability and stability of devices. These aspects of quantum wells, their impact on OLED characteristics, as well as technological challenges and solutions related to each color of emission, will be discussed in more detail in the following subsections.

4.1. Blue OLEDs using “Quantum Well” technology

The competitive performance of OLED displays and state-of-the-art OLED lighting systems is determined by the energy efficiency and lifespan of red, green, and blue (RGB) organic emitting devices [69, 70]. The emission spectrum of white light is formed by a continuous combination of red, green, and blue emission spectra. However, it should be noted that the quality of blue emission and the reliability of blue organic photodiodes remain a significant issue. The high energy of blue emission negatively affects the longevity of OLEDs due to the rapid degradation of the emissive material [71]. Additionally, these devices suffer from a rapid decline in OLED efficiency under high-brightness operation [72]. Addressing these and several other issues requires new comprehensive solutions, including developing and synthesizing basic materials and utilizing effective architectural approaches to the design of blue-emitting OLEDs.

The performance of some blue MQW OLEDs and the analysis carried out in this subsection are given in Table 2, and their energy diagrams are presented in Fig. 6a, b, and c.

Table 2. The electrical characteristics of blue MQW OLEDs.

Device	Current density, mA/ cm ²	Luminance, cd/ m ²	Turn-on voltage, V	Luminous efficiency max., cd/A	Quantum efficiency max., %	Ref.
A	115.75	8.312	3.5	17.99	9.08	[45]
B	88.88	8.521	3.0	19.46	10.02	
C	86.56	7.094	3.0	19.95	10.05	
D	78.88	6.856	2.5	18.24	8.72	
A	No data	6405.3	6,0	13.9	7.4	[46]
B	No data	8439.4	6,0	11.4	5.8	
C	No data	8954.4	6,0	12.5	5.8	
D	No data	10919.0	6,0	14.4	7.0	

In 2012, the authors of [17, 45] applied the QW_s technology with a charge control layer (CCL) as a component to enhance the efficiency of blue phosphorescent OLEDs based on a host-guest system, where FIrpic was used as the guest emitter metal-organic component, and mCP was the matrix component.

In [45] by S. Lee, J. Koo et al., three types of light-emitting structures based on QWs with the corresponding number of CCL were sequentially formed (Fig. 6a). The CCL with a 5 nm thickness consisted of a mixture of *p*- and *n*-type materials, namely mCP and TPBi (mCP/TPBi = 1:1). Thus, multilayer structures were developed, where the zones of radiative recombination contained triplet excitons. Their characteristics were compared with those of blue phosphorescent organic light-emitting diodes in a structure without QWs (control device A).

As shown in Table 2, device C, which involves triplet states in the radiative process, demonstrates the best values of brightness characteristics and external quantum efficiency. Additionally, the turn-on voltage of devices B, C, and D is lower than that of control device A.

The authors attribute such improvement in the characteristics of blue phosphorescent OLEDs to the effective charge and exciton confinement in CCL, high triplet energy states in mCP, and achieving balanced charge transport to the radiative recombination zone using an ambipolar CCL. Similar conclusions were also reached by the authors in [17], where they published high-efficiency blue phosphorescent OLEDs with a multiple quantum well structure ITO/MoO₃/NPB/[TCTA/mCP:FIrpic]_n/TmPyPB/LiF/Al (*n* = 1, 2, 3, 4 is the well number, and the corresponding device is defined as device 1, 2, 3 and 4), like to the structure of the previous study. Regarding the differences in the structures of blue phosphorescent OLEDs on quantum wells, in [17], among other transport layers used, a hole-conducting thin film of TCTA was used as CCL. This study applied a similar approach to the one presented in the previous work to investigate the influence of the number of quantum wells. The best results were achieved in the optimized device with two quantum wells, where the maximum external quantum efficiency (EQE) reached 20.31%, and the current efficiency and luminous efficiency corresponded to 40.31 cd/A and 30.14 lm/W, respectively.

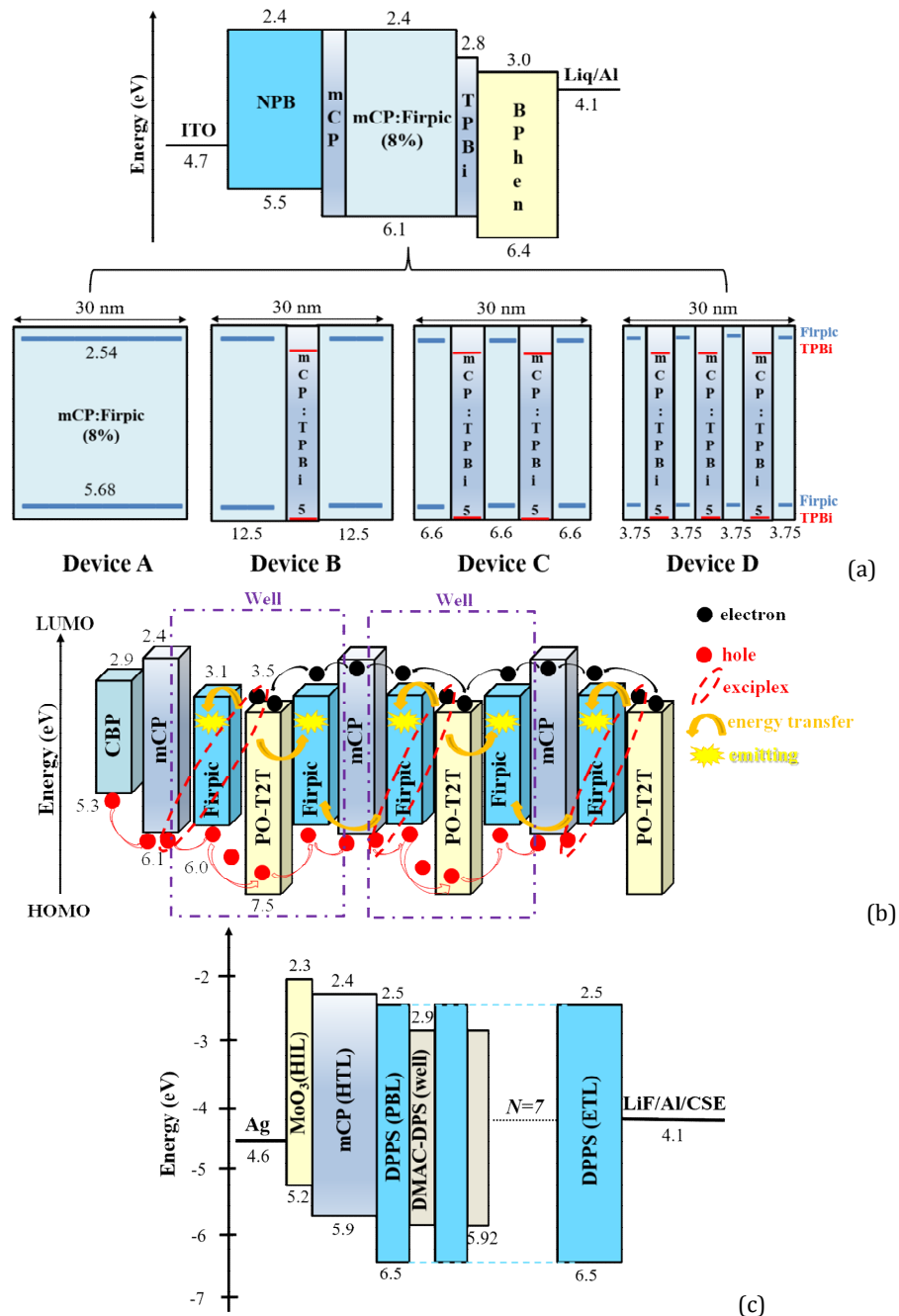


Fig. 6. The energy level diagrams of blue MQW OLEDs of the (a) devices A, B, C, and D [45] [Used with permission of Springer Nature BV, from "Effect of triplet multiple quantum well structures on the performance of blue phosphorescent organic light-emitting diodes. Lee, S., Koo, J., Hyung, G., Lim, D., Lee, D., Lee, K., Yoon, S., Kim, W., Kim, Y. 7(1), 23 Nanoscale Research Letters, (2012)". Permission conveyed through Copyright Clearance Center, Inc.]; (b) device D [46] [Used with permission of Elsevier Science &Technology Journals, from "Stabilized Huang-Rhys factor in non-doped exciplex-based Firpic phosphorescent organic light emitting diodes via quantum well-like multiple emissive layer structure and investigation of carrier behaviors by transient electroluminescence. Hu, B., Lü, Z., Tang, Z., Wu, Y., Ji, W., Wang, J. 123, 106919, Organic Electronics, (2023)". Permission conveyed through CCC Marketplace]; and (c) TADF-TEOLED [47] [Used with permission of Elsevier Science &Technology Journals, from "Cavity-suppressing electrode integrated with multi-quantum well emitter: A universal approach toward high-performance blue TADF top emission OLED. Jang, I.G., Murugadoss, V., Park, T.H., Son, K.R., Lee, H.J., Ren, W.Q., Yu, M.J., Kim, T.G. 14, 60, Nano-Micro Letters, (2022)". Permission conveyed through CCC Marketplace].

A comparative analysis of the light-emitting characteristics of the phosphorescent OLED MQW with $n = 2$ (Device 2) with the control OLED without QWs (Device 5) (Fig. 7a, Fig. 8a) allows to conclude that Device 2 demonstrates higher brightness and lower turn-on voltage. The authors [17] attribute the increase in brightness and decrease in turn-on voltage to the TCTA implantation in the MQW structure, which effectively improves hole injection and transport in the emissive layer (EML). Additionally, the mCP matrix can, to some extent, confine charges in the EML. Moreover, the maximum luminous efficiency of Device 2 demonstrated more than a 54.80% increase in luminous efficiency and a lower degradation during high-brightness operation compared to the control device (Device 5).

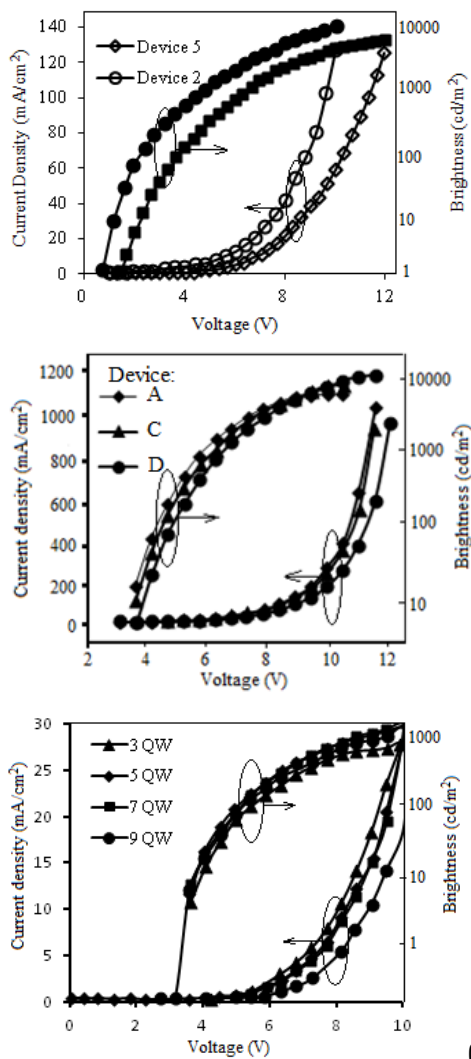


Fig. 7. Current density-voltage-brightness (J-V-B) characteristics of the: (a) MQW device (Device 2) and control device (Device 5) [17] [Reprinted with permission from "High efficiency blue phosphorescent organic light-emitting diodes with a multiple quantum well structure for reduced efficiency roll-off. Yang, X., Zhuang, S., Qiao, X., Mu, G., Wang, L., Chen, J., & Ma, D. 20(22), 24411-24417, Optics Express, (2012)" © Optica Publishing Group]; (b) QW-based devices C, D, and control device A [46] [Used with permission of Elsevier Science & Technology Journals, from "Stabilized Huang-Rhys factor in non-doped exciplex-based Firpic phosphorescent organic light emitting diodes via quantum well-like multiple emissive layer structure and investigation of carrier behaviors by transient electroluminescence. Hu, B., Lü, Z., Tang, Z., Wu, Y., Ji, W., Wang, J. 123, 106919, Organic Electronics, (2023)". Permission conveyed through CCC Marketplace]; (c) MQW devices as a function of the number of quantum wells (n) [47] [Used with permission of Elsevier Science & Technology Journals, from "Cavity-suppressing electrode integrated with multi-quantum well emitter: A universal approach toward high-performance blue TADF top emission OLED. Jang, I.G., Murugadoss, V., Park, T.H., Son, K.R., Lee, H.J., Ren, W.Q., Yu, M.J., Kim, T.G. 14, 60, Nano-Micro Letters, (2022)". Permission conveyed through CCC Marketplace].

The electroluminescent (EL) spectra of the QWs devices 1, 2, 3, and 4 are shown in Fig. 9a. All devices exhibit the main emission from Firpic with a maximum at 472 nm and a vibronic peak at 496 nm, indicating efficient energy transfer from the host material to Firpic. However, the electroluminescence intensity of vibrational transitions increases with the number of QWs, which the authors [17] attribute to the change in optical lengths in the four devices since the total thickness of the emitting layer of the four devices is different.

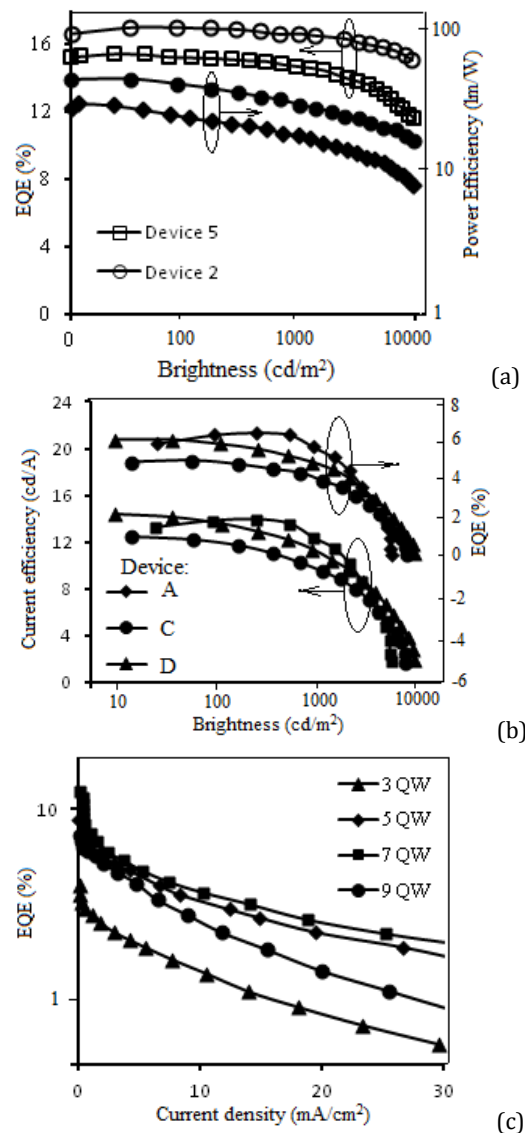
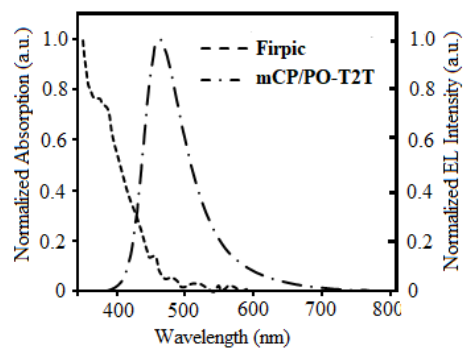


Fig. 8. The EQE - brightness - power efficiency plots of Device 2 and control Device 5 (a) [17] [Reprinted with permission from "High efficiency blue phosphorescent organic light-emitting diodes with a multiple quantum well structure for reduced efficiency roll-off. Yang, X., Zhuang, S., Qiao, X., Mu, G., Wang, L., Chen, J., & Ma, D. 20(22), 24411-24417, Optics Express, (2012)" © Optica Publishing Group]; the EQE- brightness - current efficiency curves of Devices C, D with QW structure and control Device A (b) [46] [Used with permission of Elsevier Science &Technology Journals, from "Stabilized Huang-Rhys factor in non-doped exciplex-based Firpic phosphorescent organic light emitting diodes via quantum well-like multiple emissive layer structure and investigation of carrier behaviors by transient electroluminescence. Hu, B., Lü, Z., Tang, Z., Wu, Y., Ji, W., Wang, J. 123, 106919, Organic Electronics, (2023)". Permission conveyed through CCC Marketplace]; EQE-current density plots of MQW based devices (c) [47] [Used with permission of Elsevier Science &Technology Journals, from "Cavity-suppressing electrode integrated with multi-quantum well emitter: A universal approach toward high-performance blue TADF top emission OLED. Jang, I.G., Murugadoss, V., Park, T.H., Son, K.R., Lee, H.J., Ren, W.Q., Yu, M.J., Kim, T.G. 14, 60, Nano-Micro Letters, (2022)". Permission conveyed through CCC Marketplace].

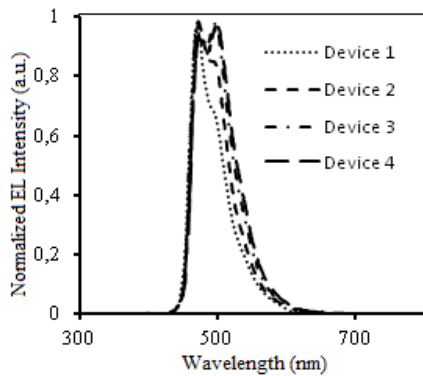
In [46], the mechanism of electroluminescence in dark-blue OLEDs was investigated (Fig. 6b), where the quantum well is the structure Firpic/PO-T2T/Firpic/mCP based on Firpic emitter. Periodically arranged layers of PO-T2T and mCP are used as spacers to separate different emission regions of the OLED. Researchers produced light-emitting devices with a traditional structure, but the different thickness of the emitter layer (Device A - ITO/MoO₃/ CBP/mCP/Firpic (0.1 nm; 0.6 nm; 1.2 nm; 2.0 nm) /PO-T2T/LiF/Al), as well as OLEDs with a quantum well structure (Device B - ITO/MoO₃/ CBP/mCP/ Firpic (0.35 nm)/PO-T2T/Firpic (0.15 nm)/mCP/Firpic (0.10 nm) /PO-T2T/LiF /Al; Device C - ITO/MoO₃/ Firpic (0.6 nm)/PO-T2T/Firpic (0.6 nm) /PO-T2T/LiF/Al; Device D - ITO /MoO₃/ CBP/mCP/ [Firpic (0.6 nm)/PO-T2T/Firpic (0.6 nm)/mCP]₂/Firpic (0.6 nm) /PO-T2T/LiF/Al), respectively.

An important aspect of the architecture of such OLEDs is the presence of a cascade of quantum wells, in which an ultra-thin layer of Firpic is positioned between the mCP and PO-T2T layers, forming an exciplex donor-acceptor intermolecular emitting complex [73],

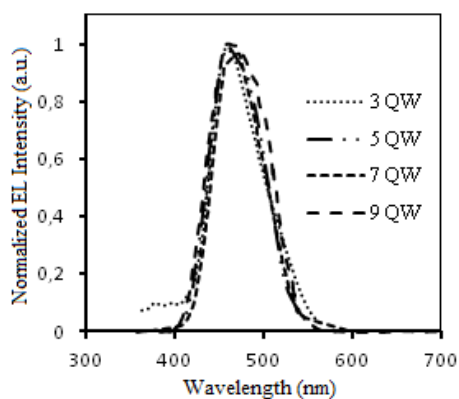
characterized by the mechanism of thermally activated delayed fluorescence (TADF). Exciplexes in OLED technology are actively used to incorporate triplet excitons into the TADF process, which fundamentally influences the properties of the OLED structure. The diffusion of the FIrpic sandwich layer into the mCP and PO-T2T films creates a host-guest system, in which FIrpic serves as the guest component. When an electric voltage is applied to such a system electroluminescent recombination can occur either by direct recombination of electrons and holes on the guest component or by starting on the mCP - PO-T2T matrix component with subsequent energy transfer from the host to FIrpic and two processes can co-occur, which is schematically depicted in Fig. 6b. The presence of an ultra-thin layer of FIrpic does not hinder the formation of an exciplex between mCP and PO-T2T [74], and the relatively wide spectral overlap of the exciplex emission with the absorption spectrum of the FIrpic emitter (Fig. 9b) enables energy transfer to FIrpic.



(a)



(b)



(c)

Fig. 9. The EL spectrum of devices 1, 2, 3, 4 (a) [17] [Reprinted with permission from "High efficiency blue phosphorescent organic light-emitting diodes with a multiple quantum well structure for reduced efficiency roll-off. Yang, X., Zhuang, S., Qiao, X., Mu, G., Wang, L., Chen, J., & Ma, D. 20(22), 24411-24417, Optics Express, (2012)" © Optica Publishing Group]; absorption of FIrpic and EL spectrum of mCP/PO-T2T exciplex (b) [46] [Used with permission of Elsevier Science &Technology Journals, from "Stabilized Huang-Rhys factor in non-doped exciplex-based FIrpic phosphorescent organic light emitting diodes via quantum well-like multiple emissive layer structure and investigation of carrier behaviors by transient electroluminescence. Hu, B., Lü, Z., Tang, Z., Wu, Y., Ji, W., Wang, J. 123, 106919, Organic Electronics, (2023)". Permission conveyed through CCC Marketplace]; EL spectra of MQW devices as a function of the number of quantum wells n (c) [47] [Used with permission of Elsevier Science &Technology Journals, from "Cavity-suppressing electrode integrated with multi-quantum well emitter: A universal approach toward high-performance blue TADF top emission OLED. Jang, I.G., Murugadoss, V., Park, T.H., Son, K.R., Lee, H.J., Ren, W.Q., Yu, M.J., Kim, T.G. 14, 60, Nano-Micro Letters, (2022)". Permission conveyed through CCC Marketplace].

The dependence of current density, brightness, current efficiency, and quantum efficiency on the voltage of QW-based devices, as presented in Fig. 7b and Fig. 8b, indicates that the current density decreases with increased FIrpic layers. According to the energy level diagram (Fig. 6b), the HOMO level difference between FIrpic and the PO-T2T layer is 1.5 eV, and the LUMO level offset between FIrpic and the mCP layer is 0.7 eV. To reach the FIrpic layers far from the anode and cathode in OLEDs, holes and electrons need to overcome additional barriers with heights of 1.5 eV and 0.7 eV, respectively. The number of barriers is proportional to the number of FIrpic layers. Therefore, a higher voltage is required to achieve the same current density for devices with more FIrpic layers. At low excitation voltages, brightness follows a similar trend, but at higher voltages exceeding 8.5 V, there is an opposite functional dependence of brightness on voltage. The authors [46] explain the nature of this dependence by tunneling charges at high voltages into the cascading of thin (2 nm) mCP and PO-T2T layers throughout the FIrpic cascade. The accumulation of a certain amount of electrons and holes at the interfaces of FIrpic/PO-T2T and mCP/FIrpic contributes to the exciton quenching in QW devices (Device B, C, D) and, as a result, exhibits lower current efficiency and greater decline in quantum efficiency at high voltages compared to control OLED (Device A). However, at higher voltages (Fig. 8b), the probability of carrier tunneling through the 2 nm layers significantly increases, and the exciton quenching by accumulated charges decreases. As a result, a wider recombination zone and a homogeneous distribution of excitons ultimately enhance device performance.

Thus, the efficiency of QW-based devices at high or ultra-high brightness surpasses that of the reference device, which is beneficial for operation in high-brightness mode. Considering that prospective dark-blue OLED emitters must meet the National Television System Committee (NTSC) standard with International Commission on Illumination (CIE) coordinates of (0.14, 0.08) [75], the high cost of rare-earth metal-based metal-organic complexes and the limited service life of phosphorescent diodes, it can be argued that blue phosphorescent organic light-emitting diodes with a quantum well structure based on FIrpic emitter do not fully meet today's needs for high-quality displays and advanced lighting systems.

In [47], an original approach of using an optimized blue emission TADF layer with QWs is proposed to create a high-efficiency top-emitting OLED with a transparent cathode electrode (TEOLED). The configuration of a TADF-TEOLED with an optically transparent cavity-suppressing Ag/WO₃/Ag (CSE) cathode electrode and MQW structures formed on a glass substrate is as follows: glass/ Ag (100 nm)/MoO₃ (2 nm)/mCP (125 nm)/[DPPS/DMAC-DPS]_n/DPPS (35 nm)/LiF/Al/CSE/DPPS. The corresponding energy level diagram of the TADF-TEOLED with an MQW structure is presented in Fig. 6c. In this structure, the MoO₃ and mCP layers are HTL. As the blue emission layer of the quantum well, a donor-acceptor TADF emitter DMAC-DPS [76] is used, surrounded on both sides by a potential barrier layer (PBL) of DPPS, which is additionally ETL.

The authors [47] noted that when optimizing the thickness of the DMAC-DPS film at the level of 2 nm, the surface roughness decreases, which leads to the formation of a homogeneous interface. In an inhomogeneous interface, due to unsatisfactory charge transfer characteristics, aggregated triplets are quenched by polarons triplet-polaron annihilation (TPA) and other triplets, causing triplet-triplet annihilation (TTA), which leads

to a decrease in device efficiency [77]. On the other hand, the smooth surface of the DMAC-DPS film during the formation of the quantum well, due to the reduction of exciton aggregation in the QW EML, on the contrary, leads to a homogeneous interface with the PBL DPPS, improving the device characteristics, particularly, EQE and brightness, and also reduces the efficiency roll-off by almost 50%.

The authors of [47] state that the device with seven quantum wells achieved a maximum EQE of 18.05%, demonstrating low-efficiency roll-off (Fig. 8c). They explain that these results can be attributed to the enhanced quantum confinement effect as well as the influence of electron-hole balance. However, increasing the number of quantum wells in the TEOLED to nine while maintaining the total device thickness reduces EQE to 10.7%. This phenomenon is associated with an increased probability of excess charge carriers tunneling through the topological narrowing of the PBL, leading to weakened exciton confinement in the quantum wells. The authors also note that all TEOLEDs with MQW structures (Fig. 7c) exhibit similar turn-on voltage levels. At the same time, the current density decreases as the number of quantum wells increases. According to their findings, an increase in the number of QWs creates more DPPS/DMAC-DPS interfaces, which, in turn, introduces defects and traps in the DMAC-DPS films and at the DPPS/DMAC-DPS interfaces, reducing the device's current density. Notably, devices with nine QWs show a significantly lower current density. Electroluminescent spectra of devices with different numbers of quantum wells, presented in Fig. 9c, confirm these patterns. The authors point out that the electroluminescence spectrum of the device with three quantum wells is characterized by a peak at 480 nm and a weak shoulder near 400 nm. They explain that the low emission efficiency in the 400 nm range is due to inefficient energy transfer between DPPS and DMAC-DPS and an insufficient number of interfaces for exciton confinement. The weak shoulder peak disappears in devices with five and seven quantum wells, which the authors associate with improved exciton confinement. In particular, devices with seven quantum wells exhibit a spectrum with a single emission peak attributed to the EML's effective charge and exciton confinement. Meanwhile, the device with nine QWs is characterized by a broader electroluminescence spectrum (Fig. 9c), similar to the spectrum of the device without quantum wells.

Therefore, based on the analysis of previous studies, the optimal selection of the number of quantum wells is crucial for achieving high device efficiency. Too few or too many quantum wells negatively affect exciton confinement and charge balance, while the optimal number ensures maximum emission efficiency.

4.2. Charge localization methods in green QW-OLEDs

As mentioned, green OLEDs with a multilayered quantum well (MQW) structure are actively researched due to their high efficiency and narrow emission spectral band. Due to their high brightness and emission stability, green OLEDs are used in portable projection systems and as light sources in lasers for medical and industrial applications. Current developments in this field include the creation of micro-OLEDs for augmented and virtual reality, where the MQW structure provides high resolution and image contrast. The manufacturing technology of green OLEDs with the MQW structure involves the layer-by-layer application of organic materials with a carefully selected band gap, which forms energy barriers for charge localization. This aspect is the efficient recombination of electrons and holes in the active zone, contributing to radiation's high brightness and stability.

In [39] the authors investigated the electroluminescent properties of green-lighting organic light-emitting diodes. The design of such devices includes a different number of QWs. The general structure of the formed OLEDs based on the Alq₃ emitter was as follows: ITO/MoO₃/[NPB/BCP]_n/NPB/Alq₃/BCP/LiF/Al. Quantum wells of this structure were formed by layers of NPB and BCP, where NPB/BCP/NPB function as HTL. Taking into account that the limiting capacity of OLEDs with MQWs structures is related to the number of periods and the QWs thickness [78-79], five OLED structures were formed by layer-by-layer thermovacuum deposition: without quantum wells ($n = 0$), single-QW ($n = 1$), double QW ($n = 2$), triple QW ($n = 3$) and quadruple-QW ($n = 4$).

A comprehensive comparative analysis of device efficiency (brightness, energy efficiency, current efficiency) showed that OLED with a double MQW structure, due to the optimal balance of carriers in the recombination zone and increased carrier recombination rate in the EML, is the most efficient among experimental OLEDs. The nature of the current density dependence of the external quantum efficiency for all devices (Fig. 10) also confirms this conclusion.

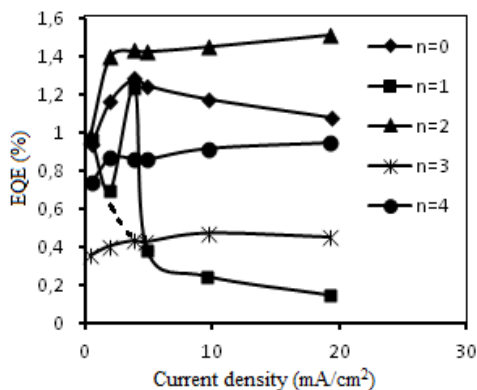


Fig. 10. EQE-current density plots of the five OLED devices [39] [Used with permission of Elsevier Science & Technology Journals, from "Efficiency enhancement of green organic light-emitting diode utilizing aromatic diamine/bathocuproine multiple quantum wells. Eskandarian, P., Fallah, H., Hajimahmoodzadeh, M., Zabolian, H., Mardani, S. J. 117, 111125, *Optical Materials*, (2021)". Permission conveyed through CCC Marketplace].

Despite an efficient green phosphorescent EML in OLEDs, insufficient dense exciton localization in the EML causes a significant decrease in the efficiency of the OLED due to the presence of triplet-triplet annihilation (TTA) and triplet-polaron annihilation (TPA) [80, 81]. Thus, to achieve higher EQE values in phosphorescent OLEDs, limiting the EML recombination zone and controlling the recombination zone (RZ) position is important. Several theoretical and empirical models have been proposed to quantify possible RZ changes. Specifically, in [82], the RZ shift is suppressed by placing additional blocking layers near the EML/HTL interface. However, it is necessary to ensure that the insertion of blocking layers does not alter the charge balance in the EML.

In [44], the mechanism of RZ localization due to the blocking of the interphase energy transfer channel was investigated for efficient phosphorescent OLEDs based on a green emitter (Ir(ppy)₃) of two types, the first type with a traditional doped host-guest system but the different thickness of the emission layer (10, 15, 20 and 30 nm), where CBP was used as matrix component (ITO/ PEDOT:PSS (40 nm)/ NPB (20 nm)/ TCTA (10 nm)/CBP : Ir(ppy)₃

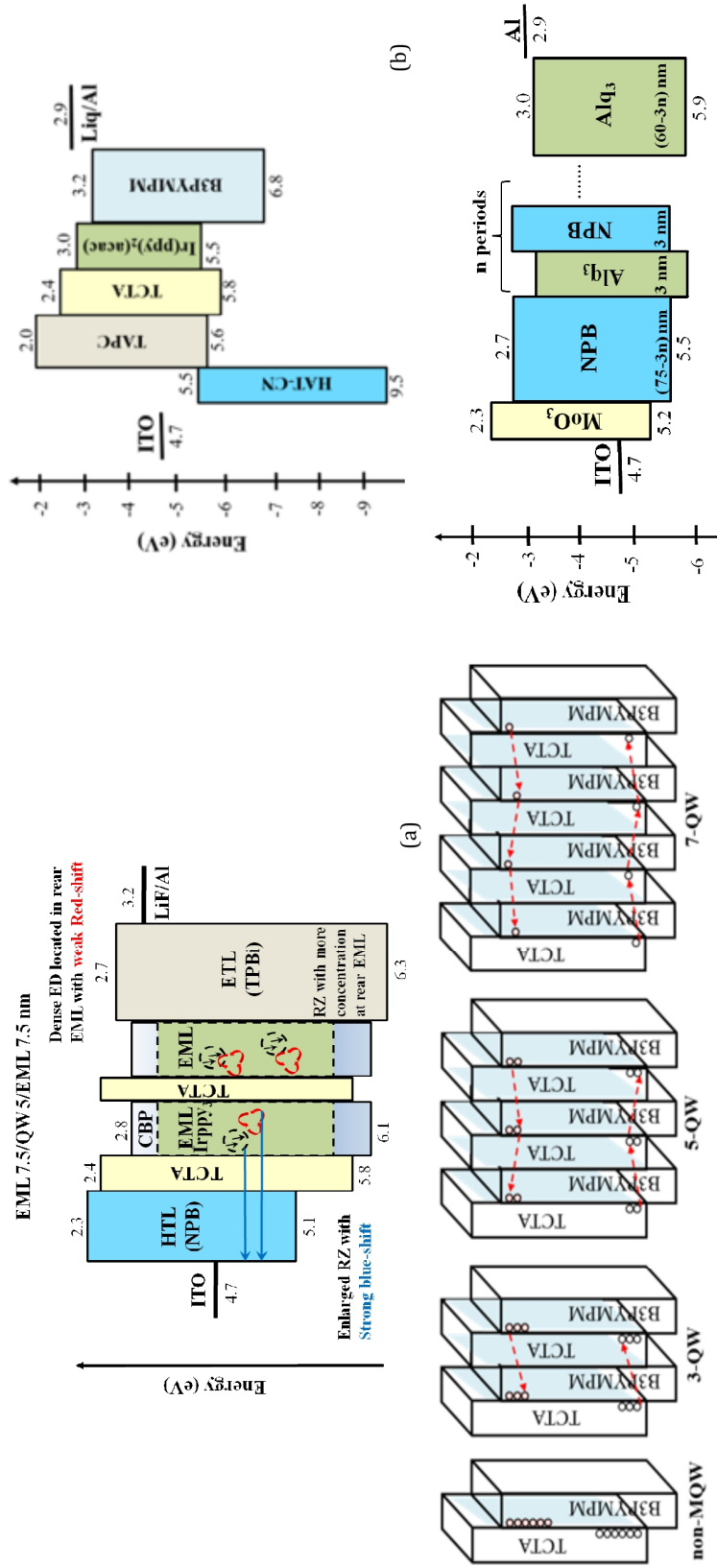


Fig. 11. The energy level diagram of the green phosphorescent OLEDs with MQW structure [44] [Used with permission of American Chemistry Society, from "Recombination zone control without sensing layer and the exciton confinement in green phosphorescent OLEDs by excluding interface energy transfer. Jesuraj, P.J., Hafeez, H., Kim, D.H., Lee, J.C., Lee, W.H., Choi, D.K., Kim, C.H., Song, M., Kim, C.S., Ryu, S.Y. 122(5), 2951-2958, Journal of Physical Chemistry C, (2018)". Copyright 2018 American Chemistry Society] (a); [50] (b); [40] [Used with permission of Elsevier Science & Technology Journals, from "The charge confinement effect of quantum-well Alq3-based OLEDs by dual-pulsed transient electroluminescence. Liu, S., Guan, M., Zhang, Y., Li, Y., Liu, X., Sun, W., Liu, C., & Zeng, Y. 419, 13-17, Optics Communications, (2018)" permission conveyed through CCC Marketplace] (c); Schematic presentation of the EML structures with non-MQW, 3-QW, 5-QW, and 7-QW (c) [50] [Used with permission of Royal Society of Chemistry, from "Management of excitons for highly efficient organic light emitting diodes with reduced triplet exciton quenching: Synergistic effects of exciplex and quantum well structure. Li, S.-H., Wu, S.-F., Wang, Y.-K., Liang, J.-J., Sun, Q., Huang, C.-C., Wu, J.-C., Liao, L.-S., Fung, M.-K. 6(2), 342-349, (2018), Journal of Physical Chemistry C, (2018)", permission conveyed through CCC Marketplace].

(10, 15, 20 and 30 nm)/ TPBi (10 nm)/LiF/ Al), and the second type of OLED, in the design of which QWs are introduced (ITO/ PEDOT:PSS (40 nm)/ NPB (20 nm)/ TCTA (10 nm)/[CBP : Ir(ppy)₃ (7.5 nm)/ TCTA (5 nm)/ CBP : Ir(ppy)₃ (7.5 nm)]/ TPBi (10 nm)/LiF/Al). RZ shift tactics were studied using a QW structure consisting of an EML/ exciton blocking layer (EBL)/EML. Ir(ppy)₃ and TCTA were used as the EML and EBL in the green phosphorescent OLEDs, respectively. TCTA was implanted as an EBL at the EML/HTL interface to maintain charge balance and RZ (Fig. 11a).

In [44], the quantum well generally consists of thin layers of organic/inorganic semiconductors, which provides a stepwise increase in energy barriers for the carriers, helping to trap excitons effectively. In addition, TCTA's ability to block electrons helps achieve a better balance of charges in the left and right EML. In this case, the RZ is formed at the border between TCTA/right EML and partially between TCTA/left EML, as shown in Fig. 11a. It is evidenced by the normalized and shift-dependent electroluminescence spectra (Fig. 12), which indicate a slight shift in the 560 nm shoulder peak due to thin (7.5 nm) EMLs and a significantly expanded recombination zone. Fig. 11a schematically represents the RZ movement in a QW- OLED structure, in which the black circle represents the RZ at the low operating voltage, and the red circle represents that of the high operating voltage. This study indicated that the RZ shifts closer to the TCTA interlayer at a higher applied potential due to the minor potential barrier between the thin 5 nm interlayer and the separated EMLs. The authors explain this because the thickness of TCTA in the structure with a quantum well is minimal; at a higher applied voltage, electrons are transferred through the TCTA layer and form excitons with holes in the left EML. In addition, the phosphorescent QW-OLED also exhibits a peak around ~420 nm (Fig. 12, inset) due to possible energy transfer and excimer formation at the TCTA/Ir(ppy)₃ interface.

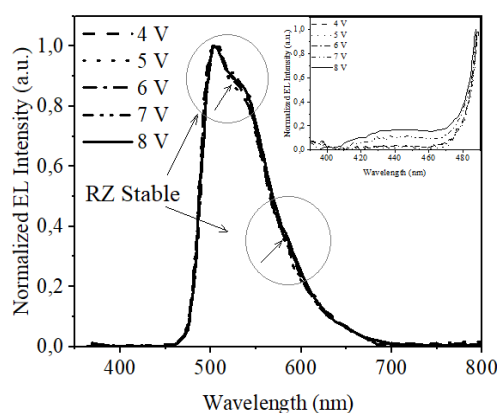


Fig. 12. The EL spectrum of green phosphorescent OLED with QW structure (Insert show the EL intensity in the QW device in the short-wavelength range from 400 to 480 nm) [44] [Used with permission of American Chemistry Society, from "Recombination zone control without sensing layer and the exciton confinement in green phosphorescent OLEDs by excluding interface energy transfer. Jesuraj, P.J., Hafeez, H., Kim, D.H., Lee, J.C., Lee, W.H., Choi, D.K., Kim, C.H., Song, M., Kim, C.S., Ryu, S.Y. 122(5), 2951-2958, Journal of Physical Chemistry C, (2018)". Copyright 2018 American Chemistry Society].

To summarize, the green phosphorescent OLEDs [44], in which the charge balance is improved and localized RZ within the EML due to the quantum well structure, demonstrated high current and quantum efficiency values of 51.93 cd/A and 14.7 % at 1000 cd/m², respectively. The overall device performances of the green phosphorescent OLEDs with different EML thicknesses and QW structures are listed in Table 3 for comparison.

Table 3. Green phosphorescent OLED performances with different types of EML structures.

EML thickness or type	Turn-on voltage, V	Current density max., mA/cm ²	Current efficiency max., cd/A	Power efficiency max., lm/W	Quantum efficiency max., %	Ref.
EML (10 nm)	-	9.2	33.14	18.35	9.5	
EML (15 nm)	-	2.3	54.43	33.11	15.39	
EML (20 nm)	-	2.7	41.76	23.13	11.87	44
EML (30 nm)	-	5.6	22.80	11.04	6.67	
EML (QW)	-	2.19	51.93	27.07	14.7	
non-MQW	2.80	4.5	83.0	93.0	25.9	
3-QW	2.80	-	84.5	94.6	26.6	50
5-QW	2.86	-	84.0	92.0	26.6	
7-QW	2.86	53	84.5	92.8	26.9	

TTA is the main reason for the decrease in OLED efficiency under operation conditions at high brightness [83, 84]. Using ultrathin emitter layers in OLED fabrication technology is believed to be an effective way to suppress TTA, most likely due to the extremely high exciton recombination zone in the ultrathin emitter layer structure [50]. The authors of [50] demonstrate the feasibility of introducing the ultrathin emitter layer between the planar intermolecular exciplex TCTA / B3PyMPM layers in the OLED structure to increase its efficiency. Ir(ppy)2acac was used as a blue phosphorescent emitter. The energy level diagram and the schematic presentation of the EML structures with different numbers of QWs (3-QW, 5-QW, and 7-QW) and without QWs (non-MQW) of the devices are shown in Fig. 11b and Fig. 11c, respectively.

Authors [50] specifically applied a cascade of quantum wells to expand the exciton recombination zone, taking into account the phenomenon of an efficiency roll-off of the devices based on quantum wells at high current densities, which occurs due to a decrease in triplet-triplet annihilation [85,86]. As the number of quantum wells increases, the density of excitons localized at each TCTA/B3PyMPM interface will decrease, and therefore, TTA will be suppressed.

The dependence of quantum efficiency on the current density of non-MQW and 7-QW devices is presented in Fig. 13. The correspondence between experimental data and theoretical calculations based on the TTA model is visualized in Fig. 13. All device performance data are summarized in Table 3. Comparing the efficiency roll-off characteristics of the device without quantum wells (non-MQW) and an OLED containing seven QWs (7-QW), using the theoretical TTA models (Fig. 13), given that the EQE = 25.9% at the minor current density of 4.5 mA/cm² for a non-MQW, and EQE = 26.9% at a current density of 53 mA/cm², it can be concluded that the dominant quenching mechanism is TTA, and such a thin design of the device structure can reduce TTA, as the efficiency roll-off was significantly reduced.

The authors of [50] experimentally established that the smallest efficiency roll-off is observed in 7-QW (a roll-off of 30.1% at 10,000 cd/m²), provided that the thickness of the TCTA/B3PyMPM layer is 3 nm. They note that the efficiencies of the non-QW, 3-QW, 5-QW, and 7-QW devices are nearly the same despite the different EML structures, confirmed by the

data in Table 3. The paper also states that the thickness increase with increasing the number of quantum wells practically does not affect the turn-on voltage of the devices (at 0.2 mA/cm^2), which increased only from 2.80 V to 2.86 V. This is explained by the high mobility of holes in TCTA ($10^{-4} \text{ cm}^2/\text{V}\cdot\text{s}$) and electrons in B3PyMPM ($10^{-5} \text{ cm}^2/\text{V}\cdot\text{s}$), as well as the optimized layer thickness of these materials, which ensures effective tunneling of charge carriers. Based on the obtained experimental data, the authors concluded that the efficiency characteristics decline directly depending on the number of quantum wells.

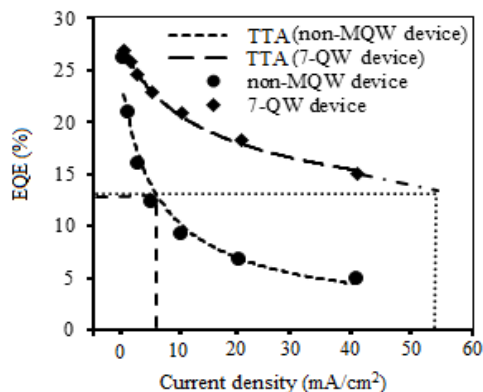


Fig. 13. EQE-Current Density plots of the non-MQW and 7-QW devices (The lines with symbols indicate the experimental data, and the two dashed lines are the fitted EQE based on the TTA model) [50] [Used with permission of Royal Society of Chemistry, from "Management of excitons for highly efficient organic light emitting diodes with reduced triplet exciton quenching: Synergistic effects of exciplex and quantum well structure. Li, S.-H., Wu, S.-F., Wang, Y.-K., Liang, J.-J., Sun, Q., Huang, C.-C., Wu, J.-C., Liao, L.-S., Fung, M.-K. 6(2), 342-349, (2018), Journal of Physical Chemistry C, (2018)". Permission conveyed through CCC Marketplace].

Transport properties, accumulation, and capture of charge carriers in OLEDs with QWs were studied in [40]. The transient electroluminescence response characteristics in OLEDs with MQW structures based on NPB/Alq₃ quantum well under dual-pulsed voltage were investigated too. For this purpose, two NPB/Alq₃ quantum-well OLEDs and a reference device with bilayer NPB/Alq₃ films were formed:

D1. ITO/MoO₃ (5 nm)/NPB (75 nm)/Alq₃ (60 nm)/LiF (1 nm)/Al (120 nm);

D2. ITO/MoO₃ (5 nm)/NPB (72 nm)/Alq₃ (3 nm)/NPB (3 nm)/Alq₃ (57 nm)/LiF (1 nm)/Al (120 nm);

D3. ITO/MoO₃ (5 nm)/NPB (69 nm)/Alq₃ (3 nm)/NPB (3 nm)/Alq₃ (3 nm)/NPB (3 nm)/Alq₃ (54 nm)/LiF (1 nm)/Al (120 nm).

A schematic energy diagram of OLEDs with multiple quantum-well structures is shown in Fig. 11d. The mechanism of transport and distribution of charge carriers in QW-OLEDs, in particular, a transient electroluminescence response signal curve driven by dual-pulsed voltage with 100 μs duration and 12 V height of the device D3 is shown in Fig. 14. As can be seen from Fig. 14, the amplitudes of the first and second transient electroluminescence responses, which are induced by a rectangular dual-pulsed voltage, are noted as S_1 and S_2 , respectively. The duration time of the pulsed voltage is repeated as T_1 , the pulse cycle as T_2 .

The researchers in [40] established that for the studied devices, the time interval required for the migration of charge carriers from the electrodes to the EML increases linearly with the increase in the number of quantum wells. This is due to the hole-type conductivity of NPB, so the electrons cannot cross the barrier at the NPB/Alq₃ interface

unhindered. Moreover, an imbalance in the mobility of charge carriers was revealed: the mobility of electrons in Alq₃ is two to three orders of magnitude lower than that of holes in NPB [87]. As a result, the main light-emitting layer is located near the cathode. Thus, as the number of quantum wells increases, the average rate at which the holes reach the EML in the heterostructure decreases.

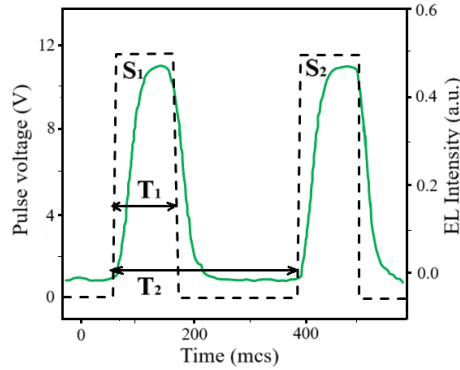


Fig. 14. Transient electroluminescence response under dual-pulsed voltage (100 μ s, 12 V) of QW-based device D [40] [Used with permission of Elsevier Science & Technology Journals, from "The charge confinement effect of quantum-well Alq₃-based OLEDs by dual-pulsed transient electroluminescence. Liu, S., Guan, M., Zhang, Y., Li, Y., Liu, X., Sun, W., Liu, C., & Zeng, Y. 419, 13-17, Optics Communications, (2018)". Permission conveyed through CCC Marketplace].

The mechanism of charge carriers' transport and distribution in QW-based device D3 under the dual-pulsed voltage was also investigated in [40] and is illustrated in Fig. 15. When a pulsed voltage is applied to the device, charge carriers are injected into the organic layers, with holes arriving first and being distributed across the two NPB barrier layers due to the higher hole mobility in NPB compared to the electron mobility in Alq₃. As a result, a significant concentration of holes accumulates in the NPB barrier layers due to the unbalanced electron injection and the 0.4 eV barrier height at the [HOMO]NPB/[HOMO]Alq₃ interface. Additionally, the holes accumulated in the NPB barrier tunnel through the 3 nm Alq₃ well N^o1. This establishes the primary recombination region at the interface between the Alq₃ well N^o1 and the NPB barrier N^o2 (Fig. 15a). The strong electric field within

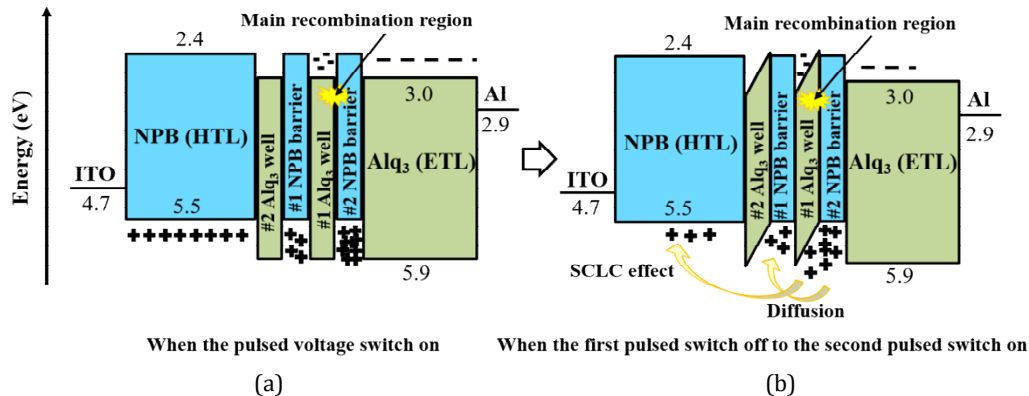


Fig. 15. Mechanism of space charge distribution and the change in the energy levels position at the boundaries of the interface [40] [Used with permission of Elsevier Science & Technology Journals, from "The charge confinement effect of quantum-well Alq₃-based OLEDs by dual-pulsed transient electroluminescence. Liu, S., Guan, M., Zhang, Y., Li, Y., Liu, X., Sun, W., Liu, C., & Zeng, Y. 419, 13-17, Optics Communications, (2018)" permission conveyed through CCC Marketplace].

the NPB barrier transforms the rectangular potential into a triangular one. When the first pulsed voltage is turned off, hole injection from the anode ceases, leading to a gradual decrease in hole concentration in the NPB HTL. The concentration gradient and triangular-shaped barrier cause holes to diffuse back into the NPB HTL from the NPB barrier №2 before the second pulse is applied (Fig. 15b). When the time interval between the two pulses is sufficiently long, there is adequate time for holes to accumulate in the NPB HTL. Consequently, a space charge limited current (SCLC) effect arises when the second pulse is applied. The accumulated space charges gradually restrict hole injection [88], resulting in $S_2 < S_1$. As the time interval between the pulses decreases, the hole concentration returning to the NPB HTL diminishes, thereby reducing the SCLC effect. Under these conditions, the intensities of the first and second pulses typically become equal. Therefore, the authors [40] found that the transient delay time increases and the fall time remains almost constant with the good numbers increasing, confirming that the exciton recombination zone is located in the Alq₃ well layer near the cathode after investigating the dual-pulsed transient EL characteristics in OLEDs with MQW structures.

Thus, research on OLEDs with MQW structure, especially for green light generation, shows significant progress in achieving high electroluminescence efficiency, reducing operating voltage, improving stability, and increasing device lifetime. The efficiency of such OLEDs is based on the confinement of charge carriers and excitons in the recombination zone, which is especially important for obtaining bright and stable green emission. Green MQW-OLEDs require detailed consideration of carrier injection and transport, which are key to ensuring high performance. Understanding the electroluminescence mechanisms in such devices plays a crucial role in optimizing their characteristics.

4.3. Red/near-infrared OLEDs with QW structure

Organic far-red and near-infrared (FR/NIR) emitters are widely used in many fields of industry and medicine [89-91]. Thus, optical absorption, light scattering, and autofluorescence are practically absent during fluorescent probing of biological objects by intense FR/NIR emission (more than 650 nm) [92]. However, it should be noted that the EQE FR/NIR OLED is inferior to the visible OLED efficiency. The fact is that in organic materials with a small energy gap (HOMO-LUMO), which are FR/NIR emitters, there is an increase in the probability of non-radiative recombination of excited states as the energy gap decreases according to the "energy gap" law [93]. The low emissivity does not contribute to the practical competitiveness of FR/NIR OLEDs, even with the advantages inherent in organic light-emitting devices, such as design flexibility, low cost, and potential biocompatibility. The main reason for the still low efficiency of FR/NIR OLEDs is triplet quenching due to triplet-triplet annihilation [94-96]. From a design perspective, triplet quenching in OLED structures can be reduced using a host-guest doping system when fabricating TADF-based OLEDs. However, as already mentioned, this approach is a complex technological challenge with often non-reproducible results, which limits the serial FR/NIR OLED production. An alternative approach to addressing this issue is using an emitter in the FR/NIR OLED design, represented by a repetitive heterostructure. In such a structure, a thin active layer (less than 10 nm, comparable to the de Broglie wavelength of charge carriers) ensures charge and exciton confinement while expanding the exciton recombination zone. This approach enables tuning the electroluminescent characteristics of FR/NIR OLEDs, driven by quantum confinement effects.

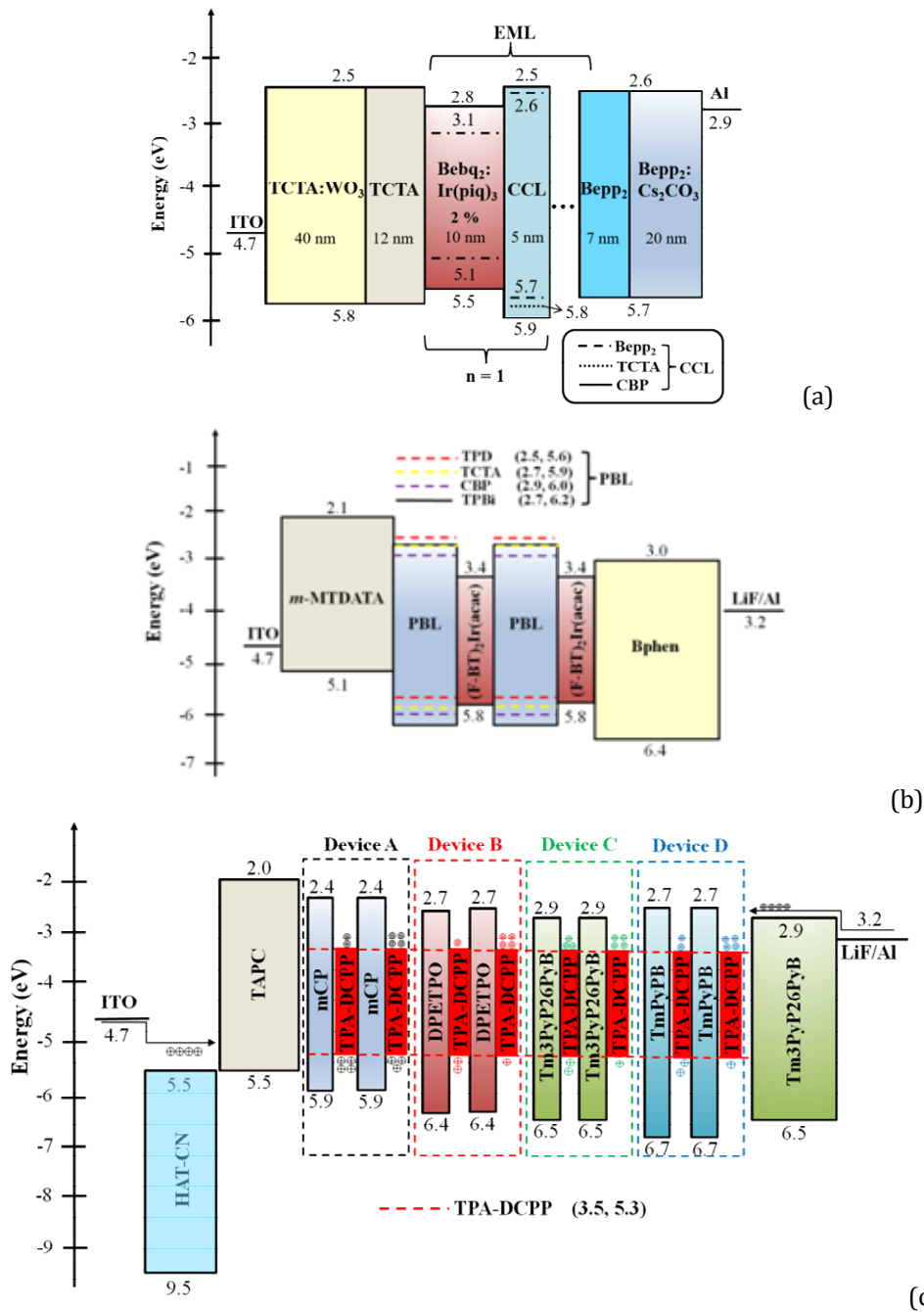


Fig. 16. The energy level diagram of the red phosphorescent OLEDs with MQW structure: (a) [51] [Used with permission of American Institute of Physics, from "Efficient multiple triplet quantum well structures in organic light-emitting devices. Park, T. J., Jeon, W. S., Choi, J. W., Pode, R., Jang, J., & Kwon, J. H. 95(10), 103303, Applied Physics Letters, (2009)". Permission conveyed through CCC Marketplace], (b) [43] [Used with permission of American Institute of Physics, from "Low-voltage, high efficiency nondoped phosphorescent organic light-emitting devices with double-quantum-well structure. Liu, S. M., Li, B., Zhang, L. M., & Yue, S. M. 98(16), 163301 (2011), Applied Physics Letters", permission conveyed through CCC Marketplace], and (c) [48] [Used with permission of American Chemistry Society, from "Efficient nondoped pure red/near-infrared TADF OLEDs by designing and adjusting double quantum wells structure. Sun, Y., Sun, W., Liu, W., Li, X., Yin, J., Zhou, L. 4(7), 3615-3622, ACS Applied Electronic Materials, (2022)". Copyright 2022 American Chemistry Society].

The authors of [51] reported a method for localizing triplet energy on the phosphorescent dopant Ir(piq)₃ in QW-OLED structures. The quantum well structure was formed using wide-bandgap transport layers hole's (TCTA) and electron's type (Bepp₂), a narrow-gap matrix (Bebq₂) doped with Ir(piq)₃, as well as CCL. Fig. 16a shows the band energy diagram of fabricated devices based on quantum wells, where n corresponds to the number of Bebq₂ layers: Ir(piq)₃/CCL (R-EL) quantum wells from one to five. Thus, including the R-EL block increased the phosphorescent OLED emission layer structure. To hold and balance holes and electrons in the EML, a 5 nm thick CCL was applied. The energy positions of TCTA, Bepp₂, Bebq₂, and Ir(piq)₃ triplets are 2.7, 2.7, 2.2, and 2.0 eV, respectively [97-100].

Since the triplet energies of the transport layers and CCL are higher than those of the host molecule, all triplet energies are confined to the emitting layers. All five devices' CIE_{x,y} chromaticity coordinates are (0.66, 0.33) at 1000 cd/m², which meets the International Commission on Illumination (CIE) requirements for red organic light-emitting devices. The various electrical parameters of the fabricated five red phosphorescent OLEDs are summarized in Table 4.

Table 4. Generalized characteristics of red phosphorescent OLEDs with MQW structure.

Well numbers (n) or PWL thickness, nm	Turn-on voltage, V	Current efficiency max., cd/A	Power efficiency max., lm/W	Quantum efficiency max., %	Ref.
n = 1	2.4	9.9	-	11.8	[51]
n = 2	2.5	12.4	-	14.8	
n = 3	2.6	11.5	-	13.6	
n = 4	2.8	10.8	-	12.8	
n = 5	3.2	7.2	-	8.6	
n = 1 Device D	2.26	14.8	16.3	-	[43]
n = 2 Device D	2.30	29.3	30.5	-	
n = 3 Device D	2.85	10.2	8.1	-	
0.5 nm Device A	2.9	15.6	15.3	14.5	[48]
1.0 nm Device A	2.8	6.0	6.1	12.0	
1.5 nm Device A	3.0	4.8	5.1	10.8	
2.5 nm Device A	2.6	2.4	2.8	6.9	
4.0 nm Device A	3.3	0.80	0.76	4.5	
5.5 nm Device A	3.1	0.74	0.73	3.3	

Shumei Liu et al. [43] reported on a highly efficient low-voltage, undoped phosphorescent OLED formed by introducing a simple triplet structure with a double quantum well, where a metal-organic complex (F-BT)₂Ir(acac) was used as a potential well layer (PWL) and an emitter in EML. Similar to the previous study [51], the authors [43] provided a CCL barrier layer in the device structure, but separately with different layers for each of the four phosphorescent OLEDs (Devices A, B, C, and D). Fig. 16b schematically depicts the energy level diagram of the fabricated devices, in which the following organic compounds were used in the CCL structures: A - TPD, B - TCTA, C - CBP, and D - TPBi, respectively. Bphen is used as an exciton/electron-blocking layer.

The triplet energy levels of TPD, TCTA, CBP, and TPBi are 2.34 eV, 2.86 eV, 2.56 eV, and 2.74 eV, respectively. All of them are higher than that of (F-BT)₂Ir(acac) at 2.25 eV, ensuring triplet excitons are held in the EML.

In the process of studying the electroluminescence spectra of phosphorescent OLEDs (Fig. 17), the authors [43] found that the emission spectra of all devices demonstrate exclusively the emission of the (F-BT)₂Ir(acac) complex with a maximum at 548 nm and a shoulder at 580 nm, indicating the complete localization of excitons in the PWL. However, in Device C, along with the strong emission of (F-BT)₂Ir(acac), a weak amplitude peak at 436 nm was recorded, corresponding to the electroluminescence of *m*-MTDATA. The authors explain this phenomenon by the drift of electrons from the PWL/EML to the HTL and their recombination with holes at the HTL/PBL interface. Device B also exhibits an *m*-MTDATA emission maximum, but only at 8 V, suggesting that electrons overcome the PWL energy barrier with increasing excitation voltage. At the same time, Device D exhibits an emission identical to Device A, regardless of voltage, with no signs of exciplex emission at the *m*-MTDATA/TPBi interface. This indicates the effective localization of electrons and excitons in the PWL/EML.

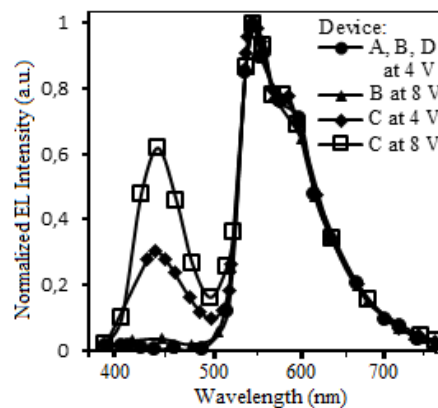


Fig. 17. Normalized EL spectra of phosphorescent OLED with QWs structure at different driving voltages [43] [Used with permission of American Institute of Physics, from "Low-voltage, high efficiency nondoped phosphorescent organic light-emitting devices with double-quantum-well structure. Liu, S. M., Li, B., Zhang, L. M., & Yue, S. M. 98(16), 163301 (2011), Applied Physics Letters". Permission conveyed through CCC Marketplace].

According to the analysis results [43], the spectral behavior of the emission in the studied OLEDs is explained as follows. As indicated in Fig. 16b, for devices A and D, the energy barriers at the PBL/PWL interface are 0.9 eV and 0.7 eV, respectively, which ensures the charge localization in the PWL/EML and the effective exciton radiative recombination. The simultaneous emission of (F-BT)₂Ir(acac) and *m*-MTDATA in Device C is explained by the bipolar transport properties of CBP and low PBL/PWL interface barriers. The energy barrier of Device B at the PBL/PWL interface is also 0.7 eV, as in Device D. However, Device B demonstrates the emission of *m*-MTDATA at high voltage in addition to the emission of (F-BT)₂Ir(acac) at low excitation voltage. The authors attribute this phenomenon to the Förster energy transfer mechanism between TCTA singlet excitons and *m*-MTDATA excitons. The turn-on voltage of Device D is the lowest and is equal to 2.3 V. In addition, this device demonstrates a high peak efficiency of 30.5 lm/W at 2.65 V and 24.5 lm/W at 3.75 V 1000 cd/m². The researchers explain such characteristics of Device D by the self-balancing effect, which is enhanced electron injection due to hole accumulation at the *m*-

MTDATA/TPBi interface. It should also be noted that besides improving electron and hole injection, the high characteristics of Device D provide the TPBi electron transport properties and shallow traps in PWL/EML. The electronic properties of phosphorescent OLEDs with different numbers of quantum wells using TPBi as PBL (Device D) are summarized in Table 4.

In recent years, there has been a trend towards increasing the FR/NIR OLED efficiency due to the TADF mechanism involvement in the ambipolar emitter layer. Due to strong spin-orbit interaction, this mechanism allows both singlet and triplet excitons involvement in the emission process during transitions, similar to phosphorescent FR/NIR emitters. Although the red-emitting organic LEDs TADF has reached an external quantum efficiency of nearly 30%, the FR/NIR OLEDs efficiency remains low - up to 10% [101, 102]. EL blue shift relative to the emitter film photoluminescence spectrum is often observed during NIR-OLEDs forming [103, 104]. A similar effect is conditioned by the choice of a matrix material with a significant dipole moment and the emitter dopant concentration. Yufu Sun et al. [48] developed a non-doped NIR TADF OLED with a double QW structure ($n = 2$) to prevent a high-energy shift in the NIR electroluminescence spectral range. The donor-acceptor emitter (TPA : DCPP) was chosen for emission in the deep red/NIR region, characterized by thermally activated delayed fluorescence [105]. The following molecular structures were used as four host materials that functioned as a PBL to confine and balance holes and electrons inside the potential well for four different devices: Device A - mCP, Device B - DPETPO, Device C - Tm3PyP26PyB and Device D - TmPyPB, respectively.

The authors used these materials since, in OLED technologies, mCP is used as a hole-transport layer or host material for phosphorescent dopants, and DPETPO, as the ambipolar organic semiconductor, functions as a matrix for phosphorescent and TADF dopants [106]. Tm3PyP26PyB and TmPyPB are electron-transport materials in organic light-emitting structures [107, 108]. The triplet energies of mCP (Device A), DPETPO (Device B), Tm3PyP26PyB (Device C), and TmPyPB (Device D) are 2.90, 3.10, 2.84, and 2.78 eV, respectively. These values are higher than in the TPA-DCPP emitter material (2.25 eV). Therefore, the confinement of triplet excitons in the PWL/EML is ensured. It should be noted that for devices with the MQWs structure, a red (excimer) shift of electroluminescence is observed, which exceeds the blue shift when the well width for narrow-band NIR TADF materials exceeds 2 nm [109]. Researchers [48] chose a potential well width of 2.5 nm based on this analysis. The structure and energy diagram of devices with double QWs are presented in Fig. 16 c. The energy positions of the HOMO levels (Device A) for TAPC and mCP (PBL) are - 5.5 and - 5.9 eV, respectively. Therefore, the interface energy barrier is low enough (0.4 eV) for holes to reach the first PWL easily. The authors [48] note that the hole movement is limited due to the high interface barrier (0.6 eV) during their transition from the first PWL to the second. The LUMO energy levels for mCP (PBL) and TPA-DCPP (PWL) are -2.4 and -3.5 eV, respectively, and the interface barrier between them reaches 1.1 eV. This leads to a low electron concentration in the second PWL, which causes electrons not to get the first PWL effectively. The authors explain that this behavior causes the formation of a negative space charge, which changes the electric field distribution in the device. It stimulates the self-balancing effect and increases the probability of charge carrier recombination [110].

The main EL performances of MQWs devices based on mCP film as PBL and TPA-DCPP film as PWL (Device A) [48] at different well widths are summarized in Table 4. Device A has the lowest turn-on voltage and better efficiency among these four devices. It should be noted that with increasing well width, the peaks of electroluminescent emission shifted towards the spectrum red region ranging from 641 to 700 nm, while the current efficiency gradually decreased. Efficiency roll-off was the fastest when the well width was 0.5 nm. In addition, the efficiency roll-off rate decreases with increasing well width. To summarize, increasing the quantum well width slows down the efficiency decline but is accompanied by a gradual decrease in the maximum efficiency of the device.

4.4. White OLEDs on QW

Recently, a trend has been towards replacing existing light sources with lighting systems based on white organic light-emitting structures (WOLED). At the same time, WOLEDs characteristics (color quality, Commission Internationale de l'Éclairage (CIE) coordinates, color rendering index, and correlated color temperature) need to be close to natural white light [111]. Although the WOLED manufacturing technology has reached commercialization, improving methods to optimize the emission color quality continues. New device architecture approaches have been created to enhance energy efficiency and color quality. It has been reported that WOLEDs with QWs structures effectively trap current carriers and excitons inside potential wells, but their emission efficiency is usually lower than that of traditional WOLED structures. Z.Y. Xie et al. and S.-H. Yang et al. obtained white organic diodes with QW structures, but the efficiency of both fabricated structures was low [112, 113]. QW-structured WOLED low efficiency is because they use exclusively fluorescent materials as emitters and the incomplete holding of charge carriers and excitons inside the EML due to using materials with an inappropriate potential barrier layer (PBL). Phosphorescent and TADF light-emitting materials must be used to utilize PBL effectively to enhance the QWs structure emission efficiency. In particular, Bo Zhao et al. [114] proposed a device architecture containing two or three phosphorescent emitters separated by blocking layers. In such a structure, electric charges tunneling through the potential barriers of the blocking layers accumulate uniformly in the potential wells, where excitons are generated, followed by electroluminescence emission in a wide spectral range. It should be noted that for such structures, matching the energy level positions of the functional layers is not critical, and the charge carriers holding inside the quantum well increase the concentration of localized excitons. This approach requires optimizing the thickness of various emitters and blocking layers and is characterized by relatively high turn-on voltages.

The authors of [49] investigated the triplet MQW structures for their incorporation into the WOLEDs architecture, where TPBi was used as the PBL, CBP was used as the host, and BCzVBi served as the blue fluorescent dopant, and Ir(ppy)₃ and Ir(piq)₃ were used as green and red phosphorescent dopants, respectively. Thus, a WOLED with TPBi as the PBL (Device A) formed a Type-I MQW structure. WOLEDs with Type II MQW structures were also formed, where Bphen or BCP was used as the PBL in WOLED instead of TPBi (Devices B and C, respectively).

In total, three MQW WOLEDs were fabricated using different semiconductors as PBLs and a reference device with the traditional three-layer structure without PBL: Device A - ITO/MoO₃ (5 nm)/CBP (20 nm)/CBP: 10% BCzVBi (5 nm)/ TPBi (2 nm)/CBP: 5% Ir(ppy)₃

(4 nm)/ TPBi (2 nm)/CBP: 4% Ir(piq)₃ (4 nm)/ TPBi (2 nm)/Bphen (45 nm)/LiF (1 nm)/Al (100 nm); Device B - ITO/MoO₃ (5 nm)/CBP (20 nm)/CBP: 10% BCzVBi (5 nm)/ Bphen (2 nm)/CBP: 5% Ir(ppy)₃(4 nm)/ Bphen (2 nm)/CBP: 4% Ir(piq)₃ (4 nm)/ Bphen (2 nm)/Bphen (45 nm)/LiF (1 nm)/Al (100 nm); Device C - ITO/MoO₃ (5 nm)/CBP (20 nm)/CBP: 10% BCzVBi (5 nm)/ BCP (2 nm)/CBP: 5% Ir(ppy)₃(4 nm)/ BCP (2 nm)/CBP: 4% Ir(piq)₃ (4 nm)/ BCP (2 nm)/Bphen (45 nm)/LiF (1 nm)/Al (100 nm); Reference device - ITO/MoO₃ (5 nm)/CBP (20 nm)/CBP: 10% BCzVBi (5 nm)/ CBP: 5% Ir(ppy)₃(4 nm)/ CBP: 4% Ir(piq)₃ (4 nm)/ Bphen (45 nm)/LiF (1 nm)/Al (100 nm). The corresponding schematic energy levels diagram of the WOLEDs with MQW structure is shown in Fig. 18.

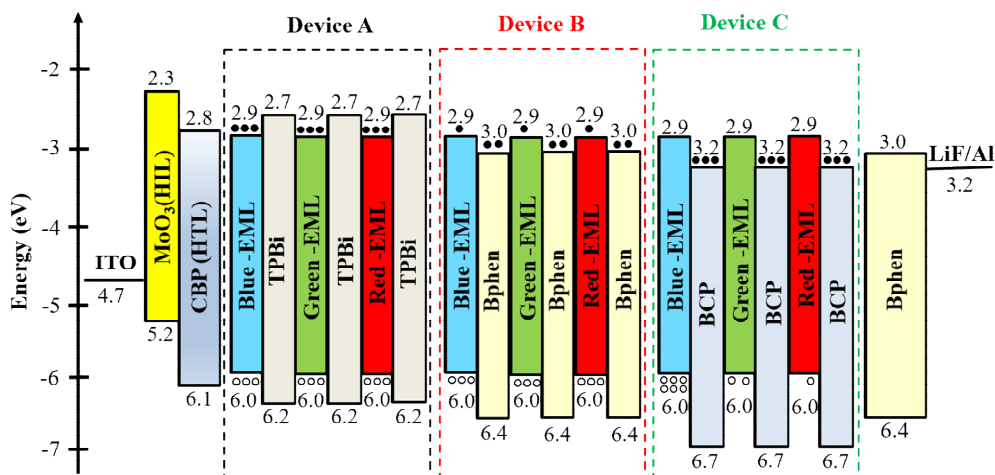


Fig. 18. The energy level diagram of the white OLEDs with MQW structure (Black balls represent electrons, and white balls are holes) [49] [Used with permission of Springer-Verlag New-York, from "The influence of type-I and type-II triplet multiple quantum well structure on white organic light-emitting diodes. Zhao, B., Su, Z., Li, W., Chu, B., Jin, F., Yan, X., Zhang, T., Zhang, F., Fan, D., Gao, Y., Wang, J., Pi, H., & Zhu, J. 8(1), 529, *Nanoscale Research Letters*, (2013)". Permission conveyed through CCC Marketplace].

It should be underlined that the Type I MQW structure is defined as a molecule with a narrow bandgap placed in a matrix formed by a wide-gap material. The injected carriers are localized between the LUMO and HOMO energy levels of the narrow-band gap molecule in such a structure. The LUMO/HOMO energy levels of both materials in the Type II MQW structure are located in a checkerboard order, and the charge carriers are placed on different molecules.

Table 5 summarizes the EL performances of all fabricated WOLEDs. The nature of the current density dependence of the current efficiency and power efficiency for all devices is depicted in Fig. 19.

Table 5. EL characteristics of WOLEDs with MQW structure.

Device	Turn-on voltage, V	Current efficiency max., cd/A	Power efficiency max., lm/W	CIE at 10V (x, y)	Ref.
Reference device	3.52	10.7	5.5	(0.38, 0.45)	
Device A	3.56	16.4	8.3	(0.32, 0.45)	[49]
Device B	3.76	11.0	4.4	(0.32, 0.45)	
Device C	3.82	8.1	3.5	(0.24, 0.35)	

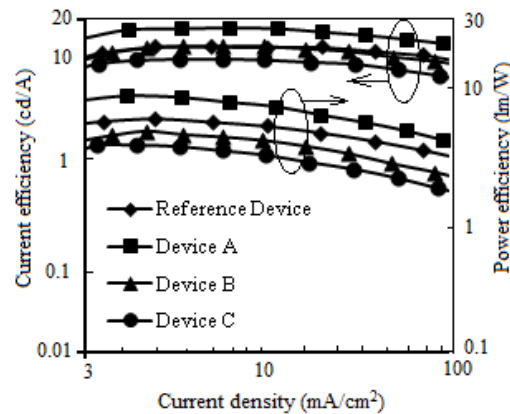


Fig. 19. CE-J-PE characteristics of all WOLEDs [49] [Used with permission of Springer-Verlag New-York, from "The influence of type-I and type-II triplet multiple quantum well structure on white organic light-emitting diodes. Zhao, B., Su, Z., Li, W., Chu, B., Jin, F., Yan, X., Zhang, T., Zhang, F., Fan, D., Gao, Y., Wang, J., Pi, H., & Zhu, J. 8(1), 529, *Nanoscale Research Letters*, (2013)". Permission conveyed through CCC Marketplace].

A comparative analysis of the light-emitting characteristics of the MQW WOLEDs (devices A, B, C) with the control OLED without PBL (reference device) (Fig. 19, Table 5) allows us to conclude that Device A demonstrates a maximum current efficiency of 16.4 cd/A and power efficiency of 8.3 lm/W at a brightness of 1000 cd/m². The authors explain that under the action of an external electric field, electrons and holes are injected from the cathode and anode, overcoming energy barriers of 0.2 eV (Fig. 18). Due to this, charge carriers are evenly distributed in the active layers (EMLs) and recombine, forming excitons. The high triplet energy of TPBi (2.74 eV), which exceeds that of CBP (2.56 eV), Ir(ppy)₃ (2.41 eV), and Ir(piq)₃ (2.0 eV), ensures effective confinement of triplet excitons inside each EML. The authors emphasize that TPBi not only performs a transport layer function but also effectively blocks excitons, preventing their migration to adjacent EML.

As shown in Fig. 18, for Device B, the hole potential well is the EML with a 0.4 eV barrier at the [HOMO]_{EML}/[HOMO]_{Bphen} interface. Thus, the injected holes could be easily confined within the HOMO energy level of EML. At the same time, a 0.1 eV barrier at the [LUMO]_{EML}/[LUMO]_{Bphen} interface allows electrons to overcome it quickly and are distributed in EML and Bphen layers. Fewer electrons are present at the LUMO EML energy level, leading to low emissive recombination efficiency.

For Device C, the situation is similar to Device B. The energy barrier height at the [LUMO]_{EML}/[LUMO]_{BCP} interface is 0.3 eV, and electrons are confined in the LUMO energy level of BCP. At the same time, the more significant barrier (0.7 eV) at the [HOMO]_{EML}/[HOMO]_{BCP} interface leads to the hole confinement in the HOMO energy level of EML. Since electrons and holes are confined in different organic layers, the exciton dissociation probability increases, carrier recombination efficiency decreases [115], and Device C presents inferior EL performances. Therefore, the other level alignments for both [LUMO]_{EML}/[LUMO]_{PBL} and [HOMO]_{EML}/[HOMO]_{PBL} for devices A, B, and C lead to different carrier recombination distribution and efficiencies.

Another conceptual adjustment of high-purity white color and color rendering index in MQW WOLED structures with the present electroplex between Zn(4-TfmBTZ)₂ as an electron-acceptor and NPB as the electron-donor of a multilayer quantum well was proposed by Ye

Zhang et al. [41]. In this study, three types of devices were fabricated and investigated: the single-emitter layer OLED (Device A), doped OLED based on a host-guest system (Device B), and multiple-layer OLED with MQWs (Device C). The device structure with MQWs is as follows: ITO/NPB(35nm)/[Zn(4-TfmBTZ)₂ (3.0 nm)/NPB(3.0 nm)]_n/ Zn(4-TfmBTZ)₂ (30 nm)/Alq₃ (30 nm)/LiF (1.8 nm)/Al (150 nm), where n responds to the well numbers 0, 1, 2.

Device C with MQW structure demonstrates the best electroluminescent characteristics. The electroluminescence spectra of Device C with different numbers of QWs at 12 V are shown in Fig. 20a, where the EL spectra normalized at 450 nm of Zn(4-TfmBTZ)₂/NPB contains five peaks corresponding to 426, 450, 480, 518, and 557 nm, respectively. The authors attribute the first and second peaks to NPB emission and the third and fourth to Zn(4-TfmBTZ)₂ charge-trapping complexes, which are capable of directly capturing charges and thus increasing the trapped electron-hole pair recombination. The fifth peak is electroplex emission around 557 nm, characteristic only of EL, and represents a spatial cross-electron transfer from the LUMO of Zn(4-TfmBTZ)₂ to the HOMO of NPB.

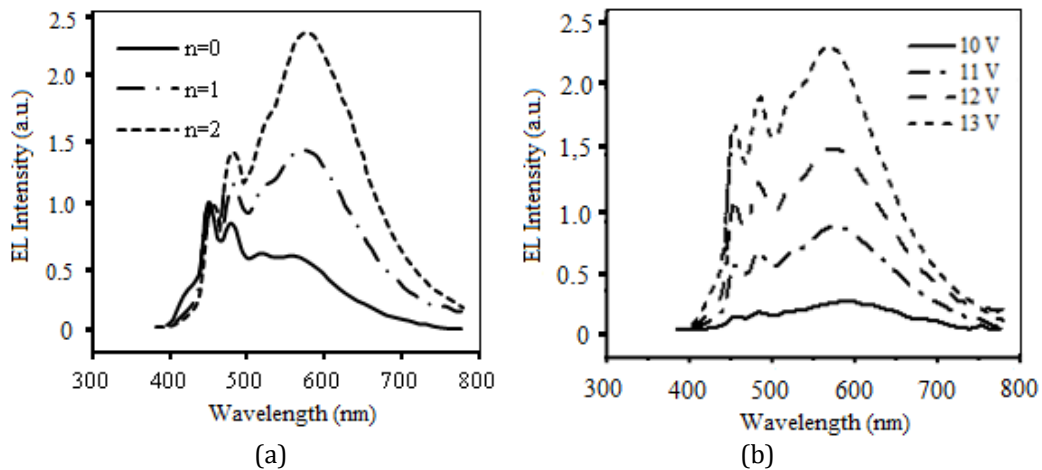


Fig. 20. EL spectra of MQW-WOLED (Device C) (a); Voltage-dependent EL spectra of Device C with $n=1$ (b) [41] [Used with permission of Springer-Verlag New-York, from "The characterization of electroplex generated from the interface between 2-(4-trifluoromethyl-2-hydroxyphenyl)benzothiazole] zinc and N,N'-diphenyl-N,N'-bis(1-naphthyl)-(1,1'-biphenyl)-4,4'-diamine. Zhang, Y., Hao, Y., Meng, W., Xu, H., Wang, H., Xu, B. 106(3), 709-715, Applied Physics A, (2011)". Permission conveyed through CCC Marketplace].

The electroplex emission becomes more intense with the number of NPB/ Zn(4-TfmBTZ)₂ interfaces. Due to the increased number of interfaces in the injection electrodes WOLED structure, the charge carriers are effectively confined at the NPB/Zn(4-TfmBTZ)₂ interface, where NPB as hole traps and Zn(4-TfmBTZ)₂ as electrons traps, respectively. Thus, the cross-electron transfer from LUMO of Zn(4-TfmBTZ)₂ to HOMO of NPB is improved. The contribution of Zn(4-TfmBTZ)₂ to EL relative to NPB increases with the number of interfaces. The researchers suggest a reason for this could be partial energy transfer from NPB to the Zn(4-TfmBTZ)₂ layer through the quantum well structure [42].

The EL spectra of an MQW WOLED with $n = 1$ at different driving voltages are shown in Fig. 20b. It is evident that the spectrum profile practically does not change with the increased applied voltage from 10 to 13 V. Therefore, the electroluminescence spectra of the MQWs device are not sensitive to the applied voltage. The distribution of electron-hole pairs

reaches a balance in the bulk and interfaces due to balancing blocking effects and tunneling through the barrier due to the quantum well structure.

In summary, to achieve high efficiency of WOLED, it is essential to ensure effective confinement of charge carriers and excitons inside the EML using the MQWs structure and the correct selection of key compounds for the formation of the EML by using phosphorescent and TADF materials, as well as optimizing the PBL, which provides better localization of excitons in potential wells and increases the efficiency of light emission. Another critical approach is using exciplexes to achieve white color with high purity and a high color rendering index. This method involves the combination of donor-acceptor materials, which allows the formation of effective electron pairs, which subsequently generate excitons with high efficiency. Such structures can provide radiation in a wide spectral range and significantly improve color characteristics when optimizing the thickness of the layers and barriers for retaining charge carriers.

5. Quantum wells practical application to improve the OLED characteristics

Numerous studies have shown that integrating quantum wells into the structure of OLED devices can significantly improve their efficiency, image quality, and overall performance. Recent studies have shown significant progress in this area. For example, studies by Q. Zhang et al. [76, 94] showed that using quantum wells increases the brightness of OLED displays and expands the color gamut, and work [98] confirmed that quantum wells reduce the power consumption of displays, which is important for portable devices. K. Kim et al. [11] noted that due to the reduction of heat loss, the overall energy efficiency of OLEDs is increased, and studies by J. Wang et al. [86, 109] showed that the use of quantum wells allows for reduced power consumption without lowering brightness, which is beneficial for energy-efficient displays.

Considerable attention has also been paid to image quality. T.J. Park et al. [51] demonstrated that quantum wells provide a more uniform brightness distribution across the screen area, which is critical for large TVs and advertising panels. S. Lee et al. [45] and S.-J. Zou et al. [116] found that quantum wells increase operational stability and reduce material degradation, especially for professional monitors and TVs.

Another essential advantage is reduced response time, as demonstrated in [40]. It makes quantum well-based OLED displays suitable for gaming devices and virtual reality systems and with high refresh rates.

The authors of [46] demonstrate how integrating a multiple emissive layer into the OLED design increases the external quantum yield, an essential factor in improving the overall device performance. Other studies, for example, [117], show that using quantum wells in luminescent materials improves their optical and electrical properties, leading to increased OLED efficiency.

However, quantum well technology plays a vital role in stabilizing and increasing the durability of OLEDs. The studies of U.S. Bhansali et al. [80] focus on this aspect, considering the advantages of quantum wells for carrier injection and the ability to withstand high electrical loads. This is important for extending the lifetime of devices, especially in the context of the latest requirements for efficiency and stability under long-term use. D. Zhao et al. [118] also reveal the energy transfer mechanisms in multilayer quantum wells, which provide additional stability for OLEDs during long-term operation.

One of the key aspects of using quantum wells is the ability to fine-tune the color of OLED emission. As R. Pan et al. [119] noted, quantum wells allow for precise color correction, providing flexibility in the choice of color parameters. This is especially important for modern display technologies, where high color accuracy is required. A prominent example is the development of quantum-well OLED displays, which achieve higher color accuracy and brightness levels, making them ideal for smartphones and high-end televisions. Quantum wells have also been used to develop highly efficient and stable OLED lighting solutions, which are crucial for energy-saving applications. For example, quantum-enhanced OLEDs are used in automotive lighting, providing brighter, more energy-efficient headlights [120].

In addition, quantum wells have shown potential in flexible wearable electronics. Researchers have successfully incorporated quantum wells into flexible OLED displays that maintain high performance even under mechanical stress [121]. This progress is significant for developing next-generation wearable devices like smartwatches and foldable smartphones. In the medical field, quantum well-based OLEDs are being investigated for use in bio-integrated devices, such as flexible sensors and diagnostic tools, due to their excellent performance and biocompatibility [122].

Thus, recent studies confirm the promise of quantum wells for improving various OLED characteristics, such as efficiency, stability, color fidelity, and applicability in flexible and wearable devices. Quantum wells are becoming integral to OLED technology innovations, opening new opportunities for more robust, high-performance devices.

6. Conclusion

Enhancement of OLED efficiency is a complex, multifaceted challenge. Thus, the OLED device efficiency can increase or decrease depending on the electroluminescence mechanisms natures inherent in the different emitters that this OLED contains. In addition to emitters, OLED performance is also affected by many other factors, including host materials, doping concentrations, fabrication methods, extraction enhancement methods, and other functional layers. Summarizing the above data, it can be noted that highly efficient devices obtained by designing OLEDs with a quantum well structure with an appropriate selection of functional layer materials and optimal thickness regulation contribute to the retention holes and electrons balancing in the emitter, which is located in the layer of the potential well. As a result, the exciton dissociation slows down, and the efficiency roll-off at high current loads is suppressed. The experimental studies presented in the review convincingly indicate that phosphorescent and TADF QWs structures with balanced charges and confined triplet excitons inside the emitter layer contribute to both the enhancement of OLED efficiency and the increase of device lifetime. The advantages of QW devices include the NIR TADF OLED with the MQWs structure. Such a design prevents the emission spectra from shifting to the high-energy region. The design strategies and mechanisms of exciton localization within QWs discussed in this review provide valuable insights into advancing OLED technology. These concepts hold significant potential for developing energy-efficient displays and lighting systems; positioning QW-based OLEDs as a cornerstone for future innovations in organic electronics.

Data availability statement

Data included in the article is available in the referenced articles.

Declaration of competing interest

The authors declare that they have no known competing financial interests or personal relationships that could have appeared to influence the work reported in this paper.

Acknowledgement

The research presented in this paper was funded by the European Union under Horizon Europe for the HELIOS project (Grant Agreement 101155017). This project has also received funding from the Research Council of Lithuania, project QUANT (Grant Agreement No S-LU-24-8), and the National Science Foundation (NSF) (Grant No OAC-2118091) in the framework of the Scientific Cooperation Program between Lithuania and Ukraine.

References

1. Wang, J., Zhang, F., Zhang, J., Tang, W., Tang, A., Peng, H., Xu, Z., Teng, F., & Wang, Y. (2013). Key issues and recent progress of high efficient organic light-emitting diodes. *Journal of Photochemistry and Photobiology C: Photochemistry Reviews*, 17, 69–104.
2. Li, D., Guo, B., Shen, Y., Li, J., & Huang, Y. (2016). Making image more energy efficient for OLED smart devices. *Mobile Information Systems*, 2016, 6575931.
3. Olajiga, O., Ani, E., Sikhakane, Z., & Olatunde, T. (2024). A comprehensive review of energy-efficient lighting technologies and trends. *Engineering Science & Technology Journal*, 5, 1097–1111.
4. Kartik, G., Sunitha, D., & Jyothi, T. (2023). Advances in solid-state lighting: A review. *Research & Development in Material Science*, 19(2), 2205–2206.
5. Blood, P. (1999). Visible-emitting quantum well lasers. In A. Miller, M. Ebrahimzadeh, & D. M. Finlayson (Eds.), *Semiconductor quantum optoelectronics* (pp. 193–211). Institute of Physics.
6. Kang, K., Byeon, I., Kim, Y. G., Choi, J., & Kim, D. (2024). Nanostructures in organic light-emitting diodes: Principles and recent advances in the light extraction strategy. *Laser & Photonics Reviews*, 18(8), 2400547.
7. Murawski, C., & Gather, M. C. (2021). Emerging biomedical applications of organic light-emitting diodes. *Advanced Optical Materials*, 9(14), 2100269.
8. Martins, P., Pereira, N., Lima, A. C., Garcia, A., Mendes-Filipe, C., Policia, R., Correia, V., & Lanceros-Mendez, S. (2023). Advances in printing and electronics: From engagement to commitment. *Advanced Functional Materials*, 33, 2213744.
9. Ahmad, S., Raushan, M. A., Gupta, H., Kattayat, S., Kumar, S., Dalela, S., Alvi, P. A., & Siddiqui, M. J. (2019). Performance enhancement of UV quantum well light emitting diode through structure optimization. *Optical and Quantum Electronics*, 51(7), 243.
10. Chen, W., Wen, X., Yang, J., Latzel, M., Patterson, R., Huang, S., Shrestha, S., Jia, B., Moss, D., Christiansen, S., & Conibeer, G. (2018). Free charges versus excitons: Photoluminescence investigation of InGaN/GaN multiple quantum well nanorods and their planar counterparts. *Nanoscale*, 10(11), 5358–5365.
11. Kim, K., Park, Y., Hyun, B. G., Choi, M., & Park, J. (2019). Recent advances in transparent electronics with stretchable forms. *Advanced Materials*, 31, 1804690.
12. Naqvi, S. M. K. A., Baig, M. F., Farid, T., Nazir, Z., Mohsan, S. A. H., Liu, Z., Cai, W., & Chang, S. (2023). Unraveling degradation processes and strategies for enhancing reliability in organic light-emitting diodes. *Nanomaterials*, 13, 3020.
13. Park, S. W., & Kim, D. (2023). Overcoming the limitation of spin statistics in organic light-emitting diodes (OLEDs): Hot exciton mechanism and its characterization. *International Journal of Molecular Sciences*, 24, 12362.
14. Meng, L., Wang, H., Wei, X., Liu, J., Chen, Y., Kong, X., Lv, X., Wang, P., & Wang, Y. (2016). Highly efficient nondoped organic light-emitting diodes based on thermally activated delayed fluorescence emitter with quantum-well structure. *ACS Applied Materials & Interfaces*, 8(32), 20955–20961.
15. Wu, S., Li, S., Sun, Q., Huang, C., & Fung, M.-K. (2016). Highly efficient white organic light-emitting diodes with ultrathin emissive layers and a spacer-free structure. *Scientific Reports*, 6(1), 25821.
16. Kar, S., Jamaludin, N. F., Yantara, N., Mhaisalkar, S. G., & Leong, W. L. (2020). Recent advancements and perspectives on light management and high performance in perovskite light-emitting diodes. *Nanophotonics*, 10(8), 2103–2143.
17. Yang, X., Zhuang, S., Qiao, X., Mu, G., Wang, L., Chen, J., & Ma, D. (2012). High efficiency blue phosphorescent organic light-emitting diodes with a multiple quantum well structure for reduced efficiency roll-off. *Optics Express*, 20(22), 24411–24417.
18. Kou, Zh., Xu, Y., Cheng, S., & Wang, X. (2016). The effect of the quantum well structure in green phosphorescent OLED with a mixed host emission interlayer. *Journal of Display Technology*, 12, 1668–1671.
19. Reinhard, E., Demarty, C.-H., & Blondé, L. (2023). Pixel value adjustment to reduce the energy requirements of display devices. *SMPTE Motion Imaging Journal*, 132(7), 10–19.

20. Xu, D., Li, X., Ju, H., Zhu, Y., & Deng, Z. (2011). A novel red organic light-emitting diode with ultrathin DCJTb and Rubrene layers. *Displays*, 32(2), 92–95.
21. Vasilopoulou, M., Fakhruddin, A., García de Arquer, F. P., Georgiadou, D., Kim, H., Yusoff, A., Gao, F., Nazeeruddin, M., Bolink, H., & Sargent, E. (2021). Advances in solution-processed near-infrared light-emitting diodes. *Nature Photonics*, 15(9), 656–669.
22. Zhao, W., Hu, X., Kong, F., Tang, J., Yan, D., Wang, J., Liu, Y., Sun, Y., Sheng, R., & Chen, P. (2024). Progress in Research on White Organic Light-Emitting Diodes Based on Ultrathin Emitting Layers. *Micromachines*, 15(5), 626.
23. Zhou, Y., Gao, H., Wang, J., Yeung, F.S.Y., Lin, S., Li, X., Liao, S., Luo, D., Kwok, H.S., Liu, B. (2023). Organic Light-Emitting Diodes with Ultrathin Emitting Nanolayers. *Electronics*, 12(14), 3164.
24. Miller, D.A.B. (1996). Optical Physics of Quantum Wells. In *Quantum Dynamics of Simple Systems* (pp. 239 - 266). Institute of Physics, London.
25. Fox, M., & Ispasoiu, R. (2006). Quantum Wells, Superlattices, and Band-Gap Engineering. In *Springer Handbooks* (pp. 1021 - 1040). Springer, Boston, MA.
26. Zhao, H., Liu, G., Zhang, J., Poplawsky, J.D., Dierolf, V., & Tansu, N. (2011). Approaches for high internal quantum efficiency green InGaN light-emitting diodes with large overlap quantum wells. *Optics Express*, 19(S4), 991 - 1007.
27. Piprek, J. (2010). Efficiency droop in nitride-based light emitting diodes. *Physica Status Solidi A*, 207(10), 2217 - 2225.
28. Zhao, H., Liu, G., Zhang, J., Arif, R.A., & Tansu, N. (2013). Analysis of internal quantum efficiency and current injection efficiency in III-nitride light emitting diodes. *Journal of Display Technology*, 9(4), 212 - 225.
29. Lin, G.-B., Meyaard, D., Cho, J., Schubert, E.F., Shim, H., & Sone, C. (2012). Analytic model for the efficiency droop in semiconductors with asymmetric carrier transport properties based on drift-induced reduction of injection efficiency. *Applied Physics Letters*, 100(16), 161106.
30. Tang, C.W., & VanSlyke, S.A. (1987). Organic electroluminescent diodes. *Applied Physics Letters*, 51(12), 913 - 915. <https://doi.org/10.1063/1.98799>
31. Burroughes, J.H., Bradley, D.D.C., Brown, A.R., Marks, R.N., Mackay, K., Friend, R.H., Burn, P.L., Holmes, A.B. (1990). Light-emitting diodes based on conjugated polymers. *Nature*, 347(6293), 539 - 541.
32. Xie, Z., Huang, J., Li, C., Liu, S., Li, Y., Wang, Y., & Shen, J. (1999). Organic multiple-quantum well white electroluminescent devices. *Synthetic Metals*, 106(1), 71 - 74.
33. Xie, Z., Huang, J., Li, C., Chen, B., Liu, S., Li, Y., Wang, Y., & Shen, J. (1999). High efficient green emission from organic multi-quantum wells structure. *Chinese Physics Letters*, 16(2), 149 - 151.
34. Sato, Y., & Kanai, H. (1994). Stability of organic electroluminescent diodes. *Molecular Crystals and Liquid Crystals*, 253, 143 - 150.
35. So, F.F., VanSlyke, S.R., Shi, Y.Q., & Steier, W.H. (1990). Quasi-epitaxial growth of organic multiple quantum well structures by organic molecular beam deposition. *Applied Physics Letters*, 56(7), 674 - 676.
36. So, F.F., & Forrest, S.R. (1991). Evidence for exciton confinement in crystalline organic multiple quantum wells. *Physical Review Letters*, 66(20), 2649 - 2652.
37. Tada, N., Tatsuha, S., Fujii, A., Ohmori, Y., & Yoshino, K. (1997). Nonlinear emission from 8-hydroxyquinoline aluminum and diamine derivative superlattice structures excited by third-harmonic-generation from Nd:YAG laser light. *Japanese Journal of Applied Physics*, 36, 421–424.
38. Chan, J., Lu, A. W., Ng, A. M. C., Djurišić, A. B., & Rakić, A. D. (2006). Organic quantum well light-emitting diodes. *Proceedings of SPIE*, 6038, 60381M.
39. Eskandarian, P., Fallah, H., Hajimahmoodzadeh, M., Zabolian, H., Mardani, S. (2021). Efficiency enhancement of green organic light-emitting diode utilizing aromatic diamine/bathocuproine multiple quantum wells. *Optical Materials*, 117, 111125.
40. Liu, S., Guan, M., Zhang, Y., Li, Y., Liu, X., Sun, W., Liu, C., & Zeng, Y. (2018). The charge confinement effect of quantum-well Alq3-based OLEDs by dual-pulsed transient electroluminescence. *Optics Communications*, 419, 13–17.
41. Zhang, Y., Hao, Y., Meng, W., Xu, H., Wang, H., Xu, B. (2011). The characterization of electroplex generated from the interface between 2-(4-trifluoromethyl-2-hydroxyphenyl)benzothiazole] zinc and N,N'-diphenyl-N,N'-bis(1-naphthyl)-(1,1'-biphenyl)-4,4'-diamine. *Applied Physics A*, 106(3), 709–715.
42. Fujita, S., Nakazawa, T., Asano, M., & Fujita, S. (2000). Comparative study of photoluminescence dynamics of tris(8-hydroxyquinoline) aluminum-based organic multilayer structures with different types of energy lineups. *Japanese Journal of Applied Physics*, 39(9R), 5301–5309.
43. Liu, S. M., Li, B., Zhang, L. M., & Yue, S. M. (2011). Low-voltage, high efficiency nondoped phosphorescent organic light-emitting devices with double-quantum-well structure. *Applied Physics Letters*, 98(16), 163301.
44. Jesuraj, P.J., Hafeez, H., Kim, D.H., Lee, J.C., Lee, W.H., Choi, D.K., Kim, C.H., Song, M., Kim, C.S., Ryu, S.Y. (2018). Recombination zone control without sensing layer and the exciton confinement in green phosphorescent OLEDs by excluding interface energy transfer. *Journal of Physical Chemistry C*, 122(5), 2951–2958.
45. Lee, S., Koo, J., Hyung, G., Lim, D., Lee, D., Lee, K., Yoon, S., Kim, W., Kim, Y. (2012). Effect of triplet multiple quantum well structures on the performance of blue phosphorescent organic light-emitting diodes. *Nanoscale Research Letters*, 7(1), 23.
46. Hu, B., Lü, Z., Tang, Z., Wu, Y., Ji, W., Wang, J. (2023). Stabilized Huang-Rhys factor in non-doped exciplex-based Fircp phosphorescent organic light emitting diodes via quantum well-like multiple emissive layer structure and investigation of carrier behaviors by transient electroluminescence. *Organic Electronics*, 123, 106919.

47. Jang, I.G., Murugadoss, V., Park, T.H., Son, K.R., Lee, H.J., Ren, W.Q., Yu, M.J., Kim, T.G. (2022). Cavity-suppressing electrode integrated with multi-quantum well emitter: A universal approach toward high-performance blue TADF top emission OLED. *Nano-Micro Letters*, 14, 60.
48. Sun, Y., Sun, W., Liu, W., Li, X., Yin, J., Zhou, L. (2022). Efficient nondoped pure red/near-infrared TADF OLEDs by designing and adjusting double quantum wells structure. *ACS Applied Electronic Materials*, 4(7), 3615–3622.
49. Zhao, B., Su, Z., Li, W., Chu, B., Jin, F., Yan, X., Zhang, T., Zhang, F., Fan, D., Gao, Y., Wang, J., Pi, H., & Zhu, J. (2013). The influence of type-I and type-II triplet multiple quantum well structure on white organic light-emitting diodes. *Nanoscale Research Letters*, 8(1), 529.
50. Li, S.-H., Wu, S.-F., Wang, Y.-K., Liang, J.-J., Sun, Q., Huang, C.-C., Wu, J.-C., Liao, L.-S., Fung, M.-K. (2018). Management of excitons for highly efficient organic light emitting diodes with reduced triplet exciton quenching: Synergistic effects of exciplex and quantum well structure. *Journal of Materials Chemistry C*, 6(2), 342–349.
51. Park, T. J., Jeon, W. S., Choi, J. W., Pode, R., Jang, J., & Kwon, J. H. (2009). Efficient multiple triplet quantum well structures in organic light-emitting devices. *Applied Physics Letters*, 95(10), 103303.
52. Li, F., Tang, H., Anderegg, J., & Shinar, J. (1997). Fabrication and electroluminescence of double-layered organic light-emitting diodes with the Al₂O₃/Al cathode. *Applied Physics Letters*, 70(10), 1233 - 1235.
53. Shimada, T., Hamaguchi, K., Koma, A., & Ohuchi, F.S. (1998). Electronic structures at the interfaces between copper phthalocyanine and layered materials. *Applied Physics Letters*, 72(15), 1869-1871.
54. Parthasarathy, G., Burrows, P.E., Khalfin, V., Kozlov, V.G., & Forrest, S.R. (1998). A metal-free cathode for organic semiconductor devices. *Applied Physics Letters*, 72(17), 2138 – 2140.
55. Huang, J., Yang, K., Xie, Z., Chen, B., Jiang, H., Liu, S. (1998). Effect of well number on organic multiple-quantum-well electroluminescent device characteristics. *Applied Physics Letters*, 73(23), 3348 – 3350.
56. Fujita, S., Nakazawa, T., Asano, M., & Fujita, S. (2000). Comparative study of photoluminescence dynamics of tris(8-hydroxyquinoline) aluminum-based organic multilayer structures with different types of energy lineups. *Japanese Journal of Applied Physics*, 39(9R), 5301–5309.
57. Fujii, A., Yoshida, M., Ohmori, Y., & Yoshino, K. (1995). Polarization anisotropy of organic electroluminescent diode with periodic multilayer structure utilizing 8-hydroxyquinoline aluminum and aromatic diamine. *Japanese Journal of Applied Physics*, 34(5B), 621–624.
58. Ohmori, Y., Fujii, A., Uchida, M., Morishima, C., & Yoshino, K. (1993). Fabrication and characteristics of 8-hydroxyquinoline aluminum/aromatic diamine organic multiple quantum well and its use for electroluminescent diode. *Applied Physics Letters*, 62(25), 3250–3252.
59. Matsushima, T., Jin, G.-H., & Murata, H. (2008). Marked improvement in electroluminescence characteristics of organic light-emitting diodes using an ultrathin hole-injection layer of molybdenum oxide. *Journal of Applied Physics*, 104, 054501.
60. Zhang, H. M., & Choy, W. C. H. (2008). Indium tin oxide modified by Au and vanadium pentoxide as an efficient anode for organic light-emitting devices. *IEEE Transactions on Electron Devices*, 55(9), 2517–2520.
61. Pommerehne, J., Vestweber, H., Tak, Y. H., & Bäessler, H. (1996). Transient electroluminescence from single- and double-layer light-emitting diodes (LEDs) based on polymer blends. *Synthetic Metals*, 76, 67–70.
62. Dastan, D., Gosavi, S. W., & Chaure, N. B. (2015). Studies on electrical properties of hybrid polymeric gate dielectrics for field-effect transistors. *Macromolecular Symposia*, 347(1), 81–86.
63. Dastan, D. (2017). Effect of preparation methods on the properties of titania nanoparticles: Solvothermal versus sol–gel. *Applied Physics A*, 123(11), 699.
64. Ayobi, A., Mirnia, S. N., Roknabadi, M. R., & Bahari, A. (2019). The effects of MoO₃/TPD multiple quantum well structures on the performance of organic light-emitting diodes (OLEDs). *Journal of Materials Science: Materials in Electronics*, 30, 3952–3958.
65. Kanai, K., Koizumi, K., Ouchi, S., Tsukamoto, Y., Sakanoue, K., Ouchi, Y., & Seki, K. (2010). Electronic structure of anode interface with molybdenum oxide buffer layer. *Organic Electronics*, 11(2), 188–194.
66. Silvaco International. (2004). *ATLAS User Manual* (1st ed.). Silvaco International.
67. Vakarchuk, I. O. (2004). *Quantum mechanics*. Lviv: Ivan Franko National University of Lviv, 784(2), 37–44.
68. Fitio, V. M. (2011). Resonance levels of the potential well created by rectangular barriers of finite height. *Visnyk of Lviv Polytechnic National University, Electronics*, 708, 173–179.
69. Tan, G., Lee, J.-H., Lin, S.-C., Zhu, R., Choi, S.-H., & Wu, S.-T. (2017). Analysis and optimization on the angular color shift of RGB OLED displays. *Optics Express*, 25(26), 33629–33642.
70. Liguori, R., Nunziata, F., Aprano, S., & Maglione, M. (2024). Overcoming challenges in OLED technology for lighting solutions. *Electronics*, 13(7), 1299.
71. Li, H.-Z., Xie, F.-M., Zhang, K., Shen, Y., Zhou, W., Li, Y.-Q., Wang, W.-J., & Tang, J.-X. (2022). Dual-channel charge transfer-based thermally activated delayed fluorescence emitter facilitating efficient and low roll-off non-doped devices. *Chemical Engineering Journal*, 436, 135234.
72. Wu, T.-L., Huang, M.-J., Lin, C.-C., Huang, P.-Y., Chou, T.-Y., Cheng, R.-W. C., Lin, H.-W., Liu, R.-S., & Cheng, C.-H. (2018). Diboron compound-based organic light-emitting diodes with high efficiency and reduced efficiency roll-off. *Nature Photonics*, 12(4), 235–240.
73. Wang, Q., Tian, Q.-S., Zhang, Y.-L., Tang, X., Liao, L.-S. (2019). High-efficiency organic light-emitting diodes with exciplex host. *Journal of Materials Chemistry C*, 7, 11329.
74. Mu, H., Jiang, Y., Xie, H. (2019). Efficient blue phosphorescent organic light emitting diodes based on exciplex and ultrathin Firpic sandwiched layer. *Organic Electronics*, 66, 195–205.

75. Lee, J.-H., Chen, C.-H., Lee, P.-H., Lin, H.-Y., Leung, M.-K., Chiu, T.-L., Lin, C.-F. (2019). Blue organic light-emitting diodes: Current status, challenge, and future outlook. *Journal of Materials Chemistry C*, 7, 5874–5888.
76. Zhang, Q.S., Tsang, D., Kuwabara, H., Hatae, Y., Li, B., Takahashi, T., Lee, S.Y., Yasuda, T., Adachi, C. (2015). Nearly 100% internal quantum efficiency in undoped electroluminescent devices employing pure organic emitters. *Advanced Materials*, 27(12), 2096–2100.
77. Rhee, S.H., Kim, C.S., Song, M., Ryu, S.Y. (2017). Correlation between interlayer thickness and device performance in blue phosphorescent organic light emitting diodes with a quantum well structure. *Organic Electronics*, 42, 343–347.
78. Qiu, Y., Gao, Y., Wang, L., Wei, P., Duan, L., Zhang, D., Dong, G. (2002). High-efficiency organic light-emitting diodes with tunable light emission by using aromatic diamine/5,6,11,12-tetraphenylnaphthacene multiple quantum wells. *Applied Physics Letters*, 81(19), 3540–3542.
79. Zhu, H., Xu, Z., Zhao, S., Zhang, F., Gao, L., Kong, C., Yan, G., Wang, Y. (2011). Study on the influences of quantum well structure on the performance of organic light emitting devices. *Displays*, 32, 102–105.
80. Bhansali, U.S., Jia, H., Lopez, M.A.Q., Gnade, B.E., Chen, W.-H., Omary, M.A. (2009). Controlling the carrier recombination zone for improved color stability in a two-dopant fluorophore/phosphor white organic light-emitting diode. *Applied Physics Letters*, 94(20), 203501.
81. Song, W., Kim, T., Lee, Y., Lee, J.Y. (2017). A stepwise energy level doping structure for improving the lifetime of phosphorescent organic light-emitting diodes. *Journal of Materials Chemistry C*, 5(16), 3948–3954.
82. Hsiao, C.-H., Chen, Y.-H., Lin, T.-C., Hsiao, C.-C., Lee, J.-H. (2006). Recombination zone in mixed-host organic light-emitting devices. *Applied Physics Letters*, 89(16), 163511.
83. Reineke, S., Walzer, K., Leo, K. (2007). Triplet-exciton quenching in organic phosphorescent light-emitting diodes with Ir-based emitters. *Physical Review B*, 75(12), 125328.
84. Setoguchi, Y., Adachi, C. (2010). Suppression of roll-off characteristics of electroluminescence at high current densities in organic light emitting diodes by introducing reduced carrier injection barriers. *Journal of Applied Physics*, 108(6), 064516.
85. Li, C., Duan, L., Zhang, D., Qiu, Y. (2015). Thermally activated delayed fluorescence sensitized phosphorescence: A strategy to break the trade-off between efficiency and efficiency roll-off. *ACS Applied Materials & Interfaces*, 7(28), 15154–15159.
86. Wang, J., Chen, J., Qiao, X., Alshehri, S. M., Ahamad, T., & Ma, D. (2016). Simple-structured phosphorescent warm white organic light-emitting diodes with high power efficiency and low efficiency roll-off. *ACS Applied Materials & Interfaces*, 8(16), 10093–10097.
87. Pinner, D. J., Friend, R. H., & Tessler, N. (1999). Transient electroluminescence of polymer light emitting diodes using electrical pulses. *Journal of Applied Physics*, 86(9), 5116–5130.
88. Niu, L., Guan, M., Chu, X., Zeng, Y., Li, Y., Zhang, Y. (2015). Transient current response characteristics in MoO₃-based organic light-emitting diodes. *The Journal of Physical Chemistry C*, 119(19), 10526–10531.
89. Qian, G., & Wang, Z. Y. (2010). Near-infrared organic compounds and emerging applications. *Chemistry - A European Journal*, 5(5), 1006–1029.
90. Zampetti, A., Minotto, A., & Cacialli, F. (2019). Near-infrared (NIR) organic light-emitting diodes (OLEDs): Challenges and opportunities. *Advanced Functional Materials*, 29, 1807623.
91. Kim, J. H., Yun, J. H., & Lee, J. Y. (2018). Recent progress of highly efficient red and near-infrared thermally activated delayed fluorescent emitters. *Advanced Optical Materials*, 6, 1800255.
92. Yeh, N. G., Wu, C.-H., & Cheng, T. C. (2010). Light-emitting diodes - their potential in biomedical applications. *Renewable and Sustainable Energy Reviews*, 14(8), 2161–2166.
93. Hu, Y., Yuan, Y., Shi, Y.-L., Li, D., Jiang, Z.-Q., & Liao, L.-S. (2018). Efficient near-infrared emission by adjusting the guest-host interactions in thermally activated delayed fluorescence organic light-emitting diodes. *Advanced Functional Materials*, 28(32), 1802597.
94. Zhang, Q., Li, B., Huang, S., Nomura, H., Tanaka, H., & Adachi, C. (2014). Efficient blue organic light-emitting diodes employing thermally activated delayed fluorescence. *Nature Photonics*, 8(4), 326–332.
95. Shimizu, M., Kaki, R., Takeda, Y., Hiyama, T., Nagai, N., Yamagishi, H., & Furutani, H. (2012). 1,4-Bis(diarylamino)-2,5-bis(4-cyanophenylethenyl)benzenes: Fluorophores exhibiting efficient red and near-infrared emissions in solid state. *Angewandte Chemie International Edition*, 124(17), 4171–4175.
96. Caspar, J. V., Kober, E. M., Sullivan, B. P., & Meyer, T. J. (1982). Application of the energy gap law to the decay of charge-transfer excited states. *Journal of the American Chemical Society*, 104(2), 630–632.
97. Jeon, W. S., Park, T. J., Kim, S. Y., Pode, R., Jang, J., & Kwon, J. H. (2009). Ideal host and guest system in phosphorescent OLEDs. *Organic Electronics*, 10(2), 240–246.
98. Kim, Y., Jeon, W. S., Park, T. J., Pode, R., Jang, J., & Kwon, J. H. (2009). Low voltage efficient simple p-i-n type electrophosphorescent green organic light-emitting devices. *Applied Physics Letters*, 94(13), 133303.
99. Tsuboi, T., Jeon, W. S., & Kwon, J. H. (2009). Observation of phosphorescence from fluorescent organic material Beq2 using phosphorescent sensitizer. *Optical Materials*, 31(12), 1755–1758.
100. Adachi, C., Baldo, M. A., & Forrest, S. R. (2000). Electroluminescence mechanisms in organic light emitting devices employing a europium chelate doped in a wide energy gap bipolar conducting host. *Journal of Applied Physics*, 87(11), 8049–8055.
101. Data, P., Pander, P., Okazaki, M., Takeda, Y., Minakata, S., Monkman, A. P. (2016). Dibenzof[a,j]phenazine-Cored Donor-Acceptor-Donor Compounds as Green-to-Red/NIR Thermally Activated Delayed Fluorescence Organic Light Emitters. *Angewandte Chemie International Edition*, 55(19), 5739–5744.

102. Ohmori, Y., Fujii, A., Uchida, M., Morishima, C., & Yoshino, K. (1993). Observation of spectral narrowing and emission energy shift in organic electroluminescent diode utilizing 8-hydroxyquinoline aluminum/aromatic diamine multilayer structure. *Applied Physics Letters*, 63(14), 1871–1873.
103. Yuan, Y., Hu, Y., Zhang, Y.-X., Lin, J.-D., Wang, Y.-K., Jiang, Z.-Q., Liao, L.-S., & Lee, S.-T. (2017). Over 10% EQE near-infrared electroluminescence based on a thermally activated delayed fluorescence emitter. *Advanced Functional Materials*, 27(26), 1700986.
104. Kim, D.-H., D'Aléo, A., Chen, X.-K., Sandanayaka, A. D. S., Yao, D., Zhao, L., Komino, T., Zaborova, E., Canard, G., Tsuchiya, Y., Choi, E., Wu, J. W., Fages, F., Brédas, J.-L., Ribierre, J.-C., & Adachi, C. (2018). High-efficiency electroluminescence and amplified spontaneous emission from a thermally activated delayed fluorescent near-infrared emitter. *Nature Photonics*, 12(2), 98–104.
105. Sun, Y., Sun, W., Zhang, D., Yin, J., Mao, M., & Zhou, L. (2023). Deep-red organic light-emitting diodes with increased external quantum efficiency and extended operational lifetime by managing the composition of mixed cohorts. *The Journal of Physical Chemistry C*, 127(39), 19378–19385.
106. Zhao, H., Liu, W., Cui, R., Feng, S., Sun, Y., Zhou, L., & Qin, D. (2022). Effects of charge mobilities and exciton blocking capabilities of charge blocking layers on the performance of organic light-emitting diodes. *Displays*, 74, 102287.
107. Zhao, X., Zhou, L., Zhu, Q., Cui, R., Cui, Y., Liu, W., Wang, J., & Mi, X. (2021). Efficient red electroluminescent devices with very low operation voltage by utilizing hole and electron transport materials as the host. *Thin Solid Films*, 717, 138474.
108. Su, S.-J., Chiba, T., Takeda, T., & Kido, J. (2008). Pyridine-containing triphenylbenzene derivatives with high electron mobility for highly efficient phosphorescent OLEDs. *Advanced Materials*, 20(11), 2125–2130.
109. Wang, J., Yu, J., Li, L., Wang, T., Yuan, K., & Jiang, Y. (2008). Low roll-off power efficiency organic light-emitting diodes consisted of nondoped ultrathin phosphorescent layer. *Applied Physics Letters*, 92(13), 133308.
110. He, G., Pfeiffer, M., Leo, K., Hofmann, M., Birnstock, J., Pudzich, R., & Salbeck, J. (2004). High-efficiency and low-voltage p-i-n electrophosphorescent organic light-emitting diodes with double-emission layers. *Applied Physics Letters*, 85(17), 3911–3913.
111. Kamalasanan, M. N., Srivastava, R., Chauhan, G., Kumar, A., Tyagi, P., & Kumar, A. (2010). Organic light-emitting diodes for white light emission. In *Organic Light Emitting Diode* (pp. 179–224).
112. Xie, Z. Y., Huang, J. S., Li, C. N., Liu, S. Y., Wang, Y., Li, Y. Q., & Shen, J. C. (1999). White light emission induced by confinement in organic multiheterostructures. *Applied Physics Letters*, 74(5), 641–643.
113. Yang, S.-H., Hong, B.-C., & Huang, S.-F. (2009). Luminescence enhancement and emission color adjustment of white organic light-emitting diodes with quantum-well-like structures. *Journal of Applied Physics*, 105(11), 113105.
114. Zhao, B., Su, Z., Li, W., Chu, B., Jin, F., Yan, X., Zhang, F., Fan, D., Zhang, T., Gao, Y., & Wang, J. (2012). High efficient white organic light-emitting diodes based on triplet multiple quantum well structure. *Applied Physics Letters*, 101(5), 053310.
115. Monkman, A. P. (2013). Singlet generation from triplet excitons in fluorescent organic light-emitting diodes. *ISRN Materials Science*, 2013, 670130.
116. Zou, S.-J., Shen, Y., Xie, F., Chen, J.-D., Li, Y., & Tang, J. (2020). Recent advances in organic light-emitting diodes: Toward smart lighting and displays. *Materials Chemistry Frontiers*, 4, 788–820.
117. Bayal, M., Chandran, N., Pilankatta, R., & Nair, S. S. (2021). Quantum wells, wires, and dots for luminescent device applications. In *Nanomaterials for Luminescent Devices, Sensors, and Bio-imaging Applications* (pp. 16). Springer.
118. Zhao, D., Song, S., Zhao, S., & Xu, Z. (2007). Energy transfer in organic multilayer quantum well structure and its application to OLEDs. *Optoelectronics Letters*, 3, 99–102.
119. Pan, R., Tang, X., Hu, Y., Zhu, H., Deng, J., & Xiong, Z. H. (2019). Extraordinary magnetic field effects mediated by spin-pair interaction and electron mobility in thermally activated delayed fluorescence-based OLEDs with quantum well structure. *Journal of Materials Chemistry C*, 1, 1–27.
120. Sun, N., Jiang, C., Li, Q., Tan, D., Bi, S., Song, J. (2020). Performance of OLED under mechanical strain: A review. *Journal of Materials Science: Materials in Electronics*, 31, 20688–20729.
121. Bauri, J., Choudhary, R. B., & Mandal, G. (2021). Recent advances in efficient emissive materials-based OLED applications: A review. *Journal of Materials Science*, 56, 18837–18866.
122. Kaushal, J. B., Raut, P., & Kumar, S. (2023). Organic electronics in biosensing: A promising frontier for medical and environmental applications. *Biosensors*, 13(11), 976.

Liliia Deva, Pavlo Stakhira, Volodymyr Fitio, Ruslana Guminilovych, Tetiana Bulavinets, Mariia Stanitska, Dmytro Volyniuk. (2025). Exploring Quantum Wells in OLED Technologies: A Comprehensive Review of Applications and Advancements. *Ukrainian Journal of Physical Optics*, 26(2), 02001 – 02047. doi: 10.3116/16091833/Ukr.J.Phys.Opt.2025.02001

Анотація. Ефективні органічні світловипромінювальні діоди (OLED), в конструкції яких структурно інтегровані квантові ями, привертають значну увагу завдяки їхній здатності забезпечувати вузьке спектральне випромінювання та високу ефективність. Особливий інтерес викликає підвищення продуктивності таких

світловипромінювальних пристроїв через впровадження у їхню архітектуру фосфоресцентних металоорганічних комплексів та матеріалів, яким притаманний механізм термоактивованої довготривалої флуоресценції. Цей підхід, завдяки сильній спін-орбітальній взаємодії, сприяє перетворенню невипромінювальних триплетних екситонів у випромінювальні синглетні екситони. У цьому огляді основна увага приділяється механізмам локалізації електрогенерованих екситонів у потенційних ямах, що дозволяє підвищити ефективність OLED шляхом збільшення яскравості випромінювання та зменшення каналів витоку екситонів через нерадіаційні процеси. Також розглядаються стратегії проєктування квантових ям для OLED, які випромінюють у синьому, зеленому, червоному, інфрачервоному та білому діапазонах. Крім того, у статті наведено аналіз практичного застосування технології квантових ям у різноманітних пристроях органічної електроніки. Огляд сучасних розробок та існуючих викликів надає всебічне уявлення про потенціал квантових ям у революціонізації OLED-технологій та окреслює майбутні тенденції в цій галузі.

Ключові слова: органічний світлодіод, квантова яма, електролюмінесценція, термічно активована довготривала флуоресценція